universität wien

MASTERARBEIT / MASTER'S THESIS

Titel der Masterarbeit / Title of the Master's Thesis

"Exploring Entorhinal Spatial Representations and Prefrontal Activations in Novel Decision-Making: An Investigation of Latent Value Spaces"

verfasst von / submitted by

Niklas Richter, BSc

angestrebter akademischer Grad / in partial fulfilment of the requirements for the degree of
Master of Science (MSc)

Wien, 2023 / Vienna 2023

Studienkennzahl lt. Studienblatt /
degree programme code as it appears on the student record sheet: A 066 840

Studienrichtung lt. Studienblatt /
degree programme as it appears on the student record sheet: Masterstudium Psychologie

Betreut von / Supervisor: Ass.-Prof. Mag. Dr. Isabella Wagner, PhD

Mitbetreut von / Co-Supervisor: Dr. Lei Zhang, PhD

Table of Contents

Abstract

With the aim to investigate the neural underpinnings of novel decision-making processes, this study builds upon recent research into the role of grid cell activity and spatial representations in abstract decision-making behavior. We enlisted seven healthy participants for a computerized binary choice task, requiring them to make decisions based on reward-related visual features. Familiar associations were established during an online training phase, and novel examples of similar features were introduced during functional magnetic resonance imaging (fMRI) sessions. This methodological framework allowed us to examine brain activity as participants extrapolated familiar associations to new examples during novel trials. We hypothesized that this cognitive process would mimic the principle of path integration within grid-cell coded spatial representations, typically observed during spatial navigation. Accordingly, we explored the influence of an abstract spatial model of feature-reward associations on the posterior medial entorhinal cortex (pmEC), expecting a specific modulation characteristic to grid cells. Additionally, we proposed hypotheses relating to activations in the orbitofrontal cortex (OFC) and the differential engagement of the ventromedial prefrontal cortex (vmPFC) based on the familiarity of decisions, considering their differential connectivity to pmEC grid cells and their pivotal roles in decision-making behavior.

Our proposed hypotheses, however, were not confirmed by our data, possibly due to heavily underpowered analysis. yet our exploratory analysis revealed intriguing activations in regions associated with entorhinal grid cells and broader spatial navigation networks, like the precuneus cortex, during novel decision trials. This hints at the potential involvement of spatial representation networks in novel abstract decision-making. While our findings provide

intriguing insights, they are preliminary and require further scientific exploration for validation and deeper understanding. Nonetheless, the robust methodology and targeted analysis of our study significantly contribute to the existing body of knowledge, strengthening the foundation for future research into the neural mechanisms that underpin decision-making processes.

Abstract (Deutsch)

Mit dem Ziel, die neuronalen Grundlagen neuartiger Entscheidungsprozesse zu erforschen, baut diese Studie auf jüngsten Forschungen zur Rolle der Aktivität von Grid Cells und räumlichen Repräsentationen im abstrakten Entscheidungsverhalten auf. Wir rekrutierten sieben gesunde Teilnehmer für eine computergestützte binäre Auswahl-Aufgabe, bei der sie Entscheidungen auf Basis von belohnungsbezogenen visuellen Merkmalen der Auswahlmöglichkeiten treffen mussten. Vertraute Assoziationen wurden während einer Online-Trainingsphase etabliert, und neue Beispiele ähnlicher Merkmale wurden während der funktionellen Magnetresonanztomographie (fMRT) eingeführt. Dieser methodische Rahmen erlaubte es uns, die Gehirnaktivität zu untersuchen, während die Teilnehmer vertraute Assoziationen auf neue Beispiele in neuartigen Entscheidungssituationen übertrugen. Wir haben die Hypothese aufgestellt, dass dieser kognitive Prozess dem Prinzip der Pfadintegration in räumlichen Repräsentationen ähnelt, die üblicherweise neuronal durch Grid Cells kodiert werden. Entsprechend untersuchten wir den Einfluss eines abstrakten räumlichen Modells von Merkmal-Belohnungs-Assoziationen auf den posterioren medialen entorhinalen Cortex (pmEC) und erwarteten eine spezifische Modulation, die für Grid Cells charakteristisch ist. Darüber hinaus stellten wir Hypothesen in Bezug auf Aktivierungen im orbitofrontalen Cortex (OFC) und

die differenzielle Beteiligung des ventromedialen präfrontalen Cortex (vmPFC) abhängig von der Vertrautheit der Entscheidungen auf, unter Berücksichtigung ihrer differenziellen Konnektivität zu Grid Cells im pmEC. Obwohl unsere Daten die Hypothesen nicht bestätigten, zeigten sie Aktivierungen im Precuneus Cortex, was auf eine Verbindung mit räumlichen Navigationsnetzwerken und Grid Cells hindeuten könnte. Dies lässt auf eine Beteiligung dieser Netzwerke an neuen, abstrakten Entscheidungsprozessen schließen. Trotz wertvoller Einblicke bedürfen unsere Ergebnisse weiterer Forschung zur Validierung. Dennoch bereichern die robuste Methodik und präzise Analyse unserer Studie das Verständnis der neuronalen Mechanismen, die den Entscheidungsprozessen zugrunde liegen, wesentlich.

Since the behaviorism era, reinforcement has been essential for understanding how organisms assign value to actions and decisions. Although this approach effectively explains habitual behavior, it does not fully account for organisms' inherent ability to assign value to entirely novel, unreinforced decisions. In this context, neuroscientists have sought to examine brain mechanisms beyond reward processing systems to explain how past experiences can be generalized to infer such values. Recent advancements in understanding the brain's spatial navigation system have led to the discovery of a particular group of neurons, known as grid cells, which may hold the key to this process. Apart from a well-established role in spatial navigation, grid cells seem to reveal themselves wherever they are looked for, recently leading up to paper titles like this – “Are Grid-Like Representations a Component of All Perception and Cognition?” (Zhang et al., 2022). Notably, the conclusion is not a straightforward yes or no. Despite the fascinating findings and theoretical frameworks that have been developed in recent years, the representational format provided by these cells (i.e the grid code) remains enigmatic in terms of its distribution and actual function in the brain, especially in non-spatial domains. As a modest contribution to this rapidly progressing scientific discussion, our study aims to investigate grid cell activity in decision-making behavior involving novel choices that necessitate drawing inferences counter to previous experience for predicting choice outcomes. By doing so, we adhere to the recent proposition of grid-coded spaces of abstract value that drive choice evaluation in some, but not all, decision-making processes. Furthermore, we explore the hypothesis that the orbitofrontal cortex (OFC) and ventromedial prefrontal cortex (vmPFC), which have a longer tradition in neuroscientific research on decision-making, may be differentially involved in either novel, grid coded, or familiar, experience-driven decisions. This

differential involvement may be due to their distinct connectivity with entorhinal cortices and their affiliated networks.

Theoretical Background

Decision making is a rather abstract term which can be defined and studied from a multitude of perspectives. However, no matter the scientific discipline or the theoretical account, decision making is on the most common note understood as the simple process of selecting one or more options from a wider range of alternatives. Historically, psychological research on decision-making has predominantly adopted perspectives inspired by economics, frequently framing decision-making in terms of adherence or deviation from normative theories of rational choice (Kahneman & Tversky, 1979). In more recent years, the integration of neuroscientific perspectives and methods has not only identified specific brain regions involved in decision-making but also increased research interest in computational and algorithmic levels (Marr, 1982) of decision making processes. This approach, rooted in animal learning theory (Rescorla & Wagner, 1972), optimal control theory (Bellman, 1957), and machine learning offers a valuable framework for modeling how decision-making strategies are adapted through ongoing experience. In recent years, researchers have made significant progress in uncovering the core brain mechanisms responsible for various computational aspects of decision-making and reinforcement learning. For instance, the discovery of the dopaminergic prediction error, initially identified by Schultz et al. (1997) and Montague et al. (1996), established a neurobiological mechanism explaining how rewards shape representations of anticipated value over time. This discovery still constitutes a seminal contribution to the field by uncovering

formal operations, such as characterised in reinforcement learning models, in neural representations of value. Such insights have greatly added interest in the nature of the neural representations that underlie our decision-making processes.

Learning Theory and Decision Making: Incorporating a Complex Reality

By integrating learning theory into the decision-making literature, longstanding issues and limitations embedded in learning paradigms were also incorporated (Behrens et al., 2018). The learning theories commonly utilized in neuroscientific investigations of decision making heavily depend on traditional behaviorist notions of strict reward-driven learning, as originally formulated in Thorndike's „Law of Effect“ (1898) or Skinner’s „About Behaviorism“ (1938), and conceptualize learning as a relatively simple mechanism of familiarization through reinforcement and trial-and-error procedure. Representations of value formed on such principles are modernly referred to as “model-free”, alluding to the fact that they do not require internal models of worldly relationships in order to drive decision making, only a prior reward history (Sutton & Barto, 1998). While model-free learning paradigms have been successful in explaining how organisms 9ptimize their decisions when faced with familiar options (O’Doherty et al., 2003), in terms of forming habitual responses, they fail to accommodate the ability of organisms to assign value to novel choices, as often encountered in real-world situations. This includes choices regarding novel cars, novel careers and so on, that cannot be evaluated based on prior reinforcements, yet almost always are driven by a sense of personal preference, and as such, by some representation of value.

Challenging Behaviorist Theory: The Emergence of Cognitive Maps

In line with the stringent assumptions of behaviorist theory, decision-making in novel situations would be anticipated to be random, due to the lack of prior reinforcement. However, ever since Tolman and Honzik (1930), as well as Tolman (1948), pioneered a series of spatial maze experiments, the capacity of organisms to rapidly infer and predict the value of previously unencountered decisions has been well-established, even within the constraints of animal models. For instance, when rats were subjected to extensive training within a maze containing a single path leading to reinforcement, they exhibited an immediate preference for more efficient routes upon their introduction to the environment (Tolman & Honzik, 1930). Such behavior suggests that, in addition to forming stimulus-outcome associations during the training phase, the rats had also developed a sophisticated cognitive representation of their spatial context, which allowed them to deny the reinforced impulse of the habitual decision and evaluate novel actions in terms of goal attainment. Importantly, the behavior of choosing the novel route could not be attributed to the factor of novelty alone, as only novel routes oriented towards the rewards actual location were preferred. Furthermore, Tolman and Honzik's (1930) discovery of learning through environmental exploration without active reinforcement emphasized that representations of environmental structure were formed latently, going beyond the traditional boundaries of behaviorist learning theory.

In response, the concept of the "cognitive map" was proposed, positing that animals and humans alike have the capacity to create an internal representation of the external world to simulate and assess potential actions before executing them. Accordingly, the cognitive map

hinges on the cognitive capacity to generate intricate representations of the complex relationships between diverse locations and landmarks within an environment. Furthermore, it was early assumed that animals may form cognitive maps that represent other, non-spatial types of information, such as the relationships between different objects or the sequence of actions in a given task Harlow (1938). Harlow (1938) found that rhesus monkeys, and humans (Harlow, 1949), demonstrated the ability to adapt their problem-solving strategies to new, similarly structured problems after being trained to solve specific tasks, such as finding hidden rewards within a complex apparatus. This finding implies that they had developed a "learning set" or a generalized representation of the task structure, which allowed them to transfer their existing knowledge to novel situations. In response, Harlow and Tolman both proposed the existence of a separate learning system that operates in parallel to more automatic and habitual learning processes, which is thought to be responsible for encountering novel situations and crucial in generalising past experiences onto new instances. This distinct learning system has been proposed to account for the capacity of humans and animals to engage in inference and generalization of experiences, wherein the underlying structure and principles of the environment can be applied to new problems without previous training or exposure. As a result, abstract reasoning and problem-solving obtained a greater emphasis in learning and decision-making research, shifting the focus from simple stimulus-response associations to more complex cognitive functions.

Cognitive Maps as World Models: Model-Based Learning vs Model-Free learning

In contemporary research, the distinct learning system proposed above is commonly identified as "model-based learning," which is similarly grounded in the notion that organisms can evaluate entirely novel actions through comprehensive representations (i.e., “internal models”) of task structures and external environments (Sutton & Barto, 1998; Daw et al., 2008).When expressed in computational terms within the framework of reinforcement-learning theory, these representations comprise a transition structure, which consists of a set of rules or equations that depict how the environment responds to actions; thus allowing for a more thorough evaluation of the decision space (Sutton & Barto, 1998). The significance of representing the transition structure lies in its ability to facilitate the simulation of future scenarios and the prediction of future outcomes. This capability proves particularly advantageous in situations where actions are novel or outcomes uncertain. As such, the brain's mechanism to form model-based representations is crucial to the neuroscientific understanding of novel decision making.

Model-free learning arguably belongs to the most well-understood processes within the brain. There are detailed explanations of its computational operations (Sutton & Barto, 1998; Rescorla & Wagner, 1979), neurotransmitter involvement (Schultz et al., 1997; Montague et al., 1996), and network interactions (Daw et al., 2008; Daw et al., 2005; O'Doherty et al., 2003), as well as accurate predictions of behavior derived from all these combined factors. However, the neural substrates underlying model-based learning systems remain largely unknown on all these levels. This discrepancy can to some degree be attributed to the fundamental differences between the two systems. Habitual behavior relies on relatively simple processes and

predictable patterns in response to quantifiable reinforcements, whereas model-based learning necessitates a comprehensive integration of spatial and task structures, incorporating multiple information sources that require advanced cognitive processing. Furthermore, accurately predicting behaviors based on model-based learning principles is challenging due to their innate flexibility and capacity to facilitate entirely novel actions.

Recent investigations have highlighted the possibility of some overlap in the neural substrates involved in model-based and model-free learning, as model parameters of the former have been shown to be relayed to striatal activity traditionally linked to the latter (Daw et al., 2011), thus suggesting that the two modes of learning are more integrated than thought. Nevertheless, a comprehensive understanding of the complex representations of environments and tasks generated by model-based learning cannot be solely explained by these findings. For one, the existence of latent learning (Tolman & Honzik, 1930), indicates that model-based representations are formed independently of reinforcement, thus deeming striatal activity of reward processing insufficient to explain the overall phenomenon. Furthermore, model-based representations often require the integration of multiple sources of information to construct a coherent representation of the environment and possible outcomes (Sutton & Barto, 1998). Consequently, such representations are challenging to investigate or even imagine based on solitary signals, such as the reward-prediction error. To this end, new representational formats beyond the brain's reward-processing systems, such a those known from spatial navigation, are considered to capture the complexity of model-based representations and the unique demands it places on the neural circuitry for novel decision-making (Bellmund et al., 2018).

Grid Cells: From Spatial Navigation to Predictive Mapping

It may not have been a coincidence that Tolman's ground-breaking studies investigating higher cognitive abilities in learning and decision-making focused on spatial navigation tasks. Advances in research on the neural codes underlying spatial navigation have revealed an entirely new representational format in the brain which was quickly assumed to provide valuable understanding of overall information processing in cortical networks (Moser et al., 2008). The cognitive map, once a theoretical concept derived from behavioral observations, has now been comprehensibly decoded at the brain's representational level. Specifically, several types of cells in the hippocampal formation, including place cells (O'Keefe & Dostrovsky, 1971), head direction cells (Taube et al., 1990), border cells (Solstad et al., 2008) and grid cells (Hafting et al., 2005), represent specialized aspects of a spatial environment and engage in intricate interactions to form an abstract, map-like representation of space. Grid cells, in particular, have garnered substantial attention due to their capacity to represent the underlying 2D coordinate system of the cognitive map, providing a metric for self-position, trajectory, and distance (Hafting et al., 2005). Grid cells are primarily found in the posterior-medial regions of the entorhinal cortex (EC), specifically in layers II and III, and exhibit unique firing fields, generating a hexagonal lattice that accurately mirrors the spatial layout of an individual's environment, thereby providing a reliable framework for navigation and spatial memory. (Hafting et al., 2005). Moreover, grid cell firing patterns are stable even when environmental cues are removed or distorted, allowing for navigation towards goal locations relying solely on grid cell representation (Fyhn et al., 2007; Zhang et al., 2014). This independence of external cues underlines the abstract nature of representation formed by grid cells and their ability to

capture the underlying structure of the environment independently from immediate sensory input, thereby providing a basis for abstraction and generalisation. Additionally, EC grid cells have not only been shown to underly spatial navigation, but also mental navigation where routes are visualized internally while remaining stationary in space (Horner et al., 2016; Bellmund et al., 2016; Doeller et al., 2010). Aside from putting further emphasis on abstraction within grid cell representations, this highlights a generative and predictive capability within the entorhinal grid system, crucial to planning and evaluating future actions. In this regard, Stachenfeld et al. (2017) explored potential generative aspects of grid cells employing a computational approach. Their findings revealed that grid-like firing patterns were capable of representing more than simply a Euclidean spatial metric. Rather, these patterns comprised a set of predictions pertaining to future states, contingent upon the task structure and a given set of actions. Consequently, grid cells were proposed to encode a "predictive map" for action, transcending their role as a mere spatial reference system for trajectory and self-position. The capacity to simulate novel actions within abstract representations, in conjunction with the extraordinary adaptability and flexibility of grid cell firing patterns across a variety of environments (Stensola et al., 2012), exhibits similarities to the demands imposed on model-based learning. This insight has prompted the proposal that grid cells could be essential components in the neural architecture underlying model-based learning and decision-making processes (Behrens, 2018; Park et al., 2021b). Should this proposition prove accurate, the representational format facilitated by grid cells might play a vital role in decision-making processes involving novel choices, even in context of non-spatial tasks.

Grid Cells and Cognitive Spaces: A Unified Framework for Information Processing

While grid cells have primarily evolved to represent spatial relationships during navigation, recent studies have uncovered a remarkable domain generality of grid codes. For instance, grid cells expand across multiple cognitive domains, exhibiting their distinct firing patterns in different perceptual systems, such as in olfactory (Bao et al., 2019), visual (Long et al., 2021a), and somatosensory (Long & Zhang, 2021b) information processing. Moreover, advances in fMRI data analysis, combined with observations of stable and coordinated activity among neighboring grid cell ensembles (Hafting et al., 2005; Barry et al., 2007), have enabled researchers to examine grid cell representations in massed population codes (Doeller et al., 2010), surpassing the limitations of earlier electrophysiological methods. Consequently, grid cell research has become more accessible, but also shifting its focus from invasive animal experiments to human studies, and thus expanding the focus of cognitive processes where grid cell activity is being investigated. As such, recent studies have probed the role of grid codes in higher-order cognitive domains, and, indeed, grid code has been observed in functions such as object classification and reasoning (Constantinescu et al., 2016), social cognition (Park et al., 2021a; Wagner et al., 2023) and novel decision-making (Bongioanni et al., 2021; Park et al., 2021a).

These findings have sparked growing interest in investigating grid-like responses and the communality the representational format brings across various instances. To date, only a limited number of theoretical frameworks have been put forth to explain these domain-general manifestations of grid code. One such framework suggests that grid cells represent a higher-order structure of sensory information that is distinct from immediate sensory input (Bellmund

et al., 2018; Whittington et al., 2020; Park et al., 2021b). From this perspective, entorhinal grid codes are thought to generate an abstract model of stimulus relationships that aligns with sensory modalities and immediate sensory inputs but is represented separate from it. As such, the domain generality of grid cells could be attributed to their role as a neural code for the structured representation of relational knowledge within the environment, independent of the way the environment is perceived. This idea builds on a well-known two-system view of memory-guided behavior (Ranganath & Ritchey, 2012), positioning the entorhinal cortex (EC) at a critical juncture between two distinct forms of representations. Specifically, this idea suggests that the entorhinal cortex, divided into medial and lateral portions, receives distinct inputs from two separate cortical networks: the anterior-temporal (AT) network, responsible for encoding perceptual or semantic features of sensory inputs as well as establishing familiarity-based object identities (e.g. object and facial recognition) and the posterior-medial (PM) network, responsible for encoding contextual associations defining relationships in temporal, spatial or abstract relational terms (Raganath & Ritchey, 2012). Notably, this model was developed without explicitly concentrating on grid cells and aimed to challenge the unitary concepts of episodic and declarative memory within hippocampal and medial temporal lobe structures. It offered a novel perspective on how cortical networks manage the "what" and "where" elements of memory content. According to this model, the medial entorhinal cortex (mEC), which houses the majority of grid cells, functions as a critical node in the abstract relational network for contextual associations in the posterior-medial (PM) system. This idea was proposed even before the full extent of grid cells' involvement in non-spatial domains was comprehended. The subsequent identification of grid cells throughout regions of the PM-

network (Bongioanni et al., 2021; Park et al., 2021a; Constantinescu et al., 2016; Doeller et al., 2010) could suggest that they provide a vital function in conveying abstract relational information commonly associated to the network. Specifically, it has been proposed that grid cells span "feature spaces" or “cognitive spaces“, implying that neural information processing may rely on processing sensory information within an abstract space, facilitating its organization through spatial reasoning (Bellmund et al., 2018). For instance, the concept of feature spaces proposes that the multifaceted process of sensory discrimination operates similarly to established classification algorithms, such as k-nearest neighbors (Fix & Joseph Hodges, 1951). Within this framework, data points are represented in a multivariate space, enabling the use of geometric measures like Euclidean distance for stimulus classification based on positional information. Building on a similar line of reasoning, it is suggested that the brain arranges concepts within a cognitive map, facilitating the investigation of abstract relationships in a manner analogous to navigating physical space (Bellmund et al., 2018). Constantinescu et al. (2016) investigated this notion through an experiment wherein participants learned arbitrary associations between bird-size configurations and christmas symbols. Results showed that participants structured the two dimensions of bird size variation (neck and leg length) into a 2D spatial representation, as their neural activity was modulated based on the trajectory between bird configurations in a hexagonally symmetric manner, similar to the grid code observed in spatial navigation. This finding suggests that humans might utilize grid cells for navigating abstract conceptual representations, supporting the idea that they, and the broader hippocampal-entorhinal system, can represent task-relevant dimensions of non-spatial experiences in spatial terms.

Consequently, the representational format of grid cells may enhance cognitive and behavioral flexibility by enabling the expansion of spatially organized associations into novel regions of cognitive space, thereby promoting inference and generalization. It is proposed that experience might tune grid cell representations of small spatial scale for accurate discrimination within cognitive space, while cell populations displaying larger spatial scales may reflect the processes of generalization to unfamiliar stimuli and new situations, surpassing the original constraints of actual experience (Bellmund et al., 2018). Similarly, by separating structural codes from event-specific sensory codes, neural representations of an object in one context can be inferred from activity patterns associated with other objects in different contexts, relying solely on the connections within an abstract relational space. A study by Baram et al. (2020) exemplifies this capacity. Their findings showed that entorhinal cortex activity patterns represent not only the correlational structure of stimulus-outcome associations in a learning task, but also generalize across tasks with diverse sensory stimuli, provided the latent task structure remains consistent. This highlights the entorhinal cortex's role in processing intricate relational information, going beyond sensory modalities and fostering cognitive flexibility and adaptability when encountering novelty, either between or within contexts.

Grid Cells in Novel Decision-Making: Context and Recent Discoveries

In light of the above, grid cells have recently been investigated within the context of novel decision-making. These studies have found that activity patterns in the hippocampal-entorhinal complex align with Euclidean distances between entities in multidimensional abstract task spaces, both in humans (Park et al., 2021a) and macaque monkeys (Bongioanni et al., 2021).

Specifically, these investigations discovered a spontaneous organization of value hierarchy into 2D spatial representations, as neural activity was subject to hexadirectional modulation, the characteristic signal of grid cells.

Using similar training protocols, participants or subjects in these studies completed two distinct training sets, each focusing on forming unidimensional value associations. For example, in Park et al. (2021b), human subjects associated individuals with competence versus popularity, while in Bongioanni et al. (2021), macaque monkeys linked color with reward probability and the number of dots with reward magnitude. Following this, they engaged in a novel decision-making task separate from the training tasks, which necessitated the integration of the two independent unidimensional ranks to form entirely new decisions, testing the ability of participants/monkeys to dynamically compute corresponding decision values. The results from both studies disclosed grid-like representations for trajectory in 2D abstract space during novel decisions, not only in the entorhinal cortex but also within the interconnected ventromedial prefrontal cortex (vmPFC), posterior and anterior cingulate cortex, as well as retrosplenial regions, which all are components of the posterior-medial (PM) network. Importantly, these findings were exclusive to novel, unexperienced decisions, highlighting the role of this representational format in generalizing experiences to new unseen instances and laying the foundation for current study.

Investigating the Interplay between Grid Cells and Prefrontal Regions

Although grid cells seem to be involved in the decision-making process for novel choices, integrating this finding with current knowledge presents certain challenges.

It is worth noting that the involvement of grid-coded representations in decision-making processes is not entirely clear. Only Park et al. have provided evidence for grid coding during actual value comparison. Bongioanni et al., on the other hand, observed grid coding in their experimental paradigm only during a passive viewing task, which, at the minimum, supports the role of grid coding in stimulus categorization and, at the maximum, in reasoning, similar to the findings of Constantinescu et al. (2016), but not explicitly in decision-making.Furthermore, a key question is whether the widespread grid-coded signal reflects the existence of grid cells in traditionally non-spatial areas or inherited activity from downstream engagement of the medial entorhinal cortex (mEC). Resolving these issues is crucial for understanding grid cell function in decision-making, particularly in relation to prefrontal areas, such as the OFC and vmPFC, which have long-established associations with decision-making processes. Many of the cognitive functions attributed to the entorhinal grid code in the present thesis have typically been ascribed to these prefrontal areas, including behavioral flexibility, model-based inference and generalization, as well as value representation (see Raithel & Gottfried, 2021 for an extensive review). As such, their interactions with grid-coded signals are crucial to understand, seeing that the nature and distribution of grid codes in prefrontal regions remains uncertain. While most studies have detected them in the vmPFC (Bongioanni et al., 2021; Park et al., 2021; Bao et al., 2019; Doeller et al., 2010), others have also identified them in the OFC (Constantinescu et al., 2016). Moreover, while Bongioanni et al. (2021) did neither find grid code in the OFC, nor specific responses to novel decisions, observing these only in the vmPFC, their results showed that the OFC strongly responded to value representation and comparison signals across novel

and familiar trials, indicating its continued central role in decision-making, even in the presence of grid-coded value representations for novel choices.

Importantly, the OFC, unlike the vmPFC, is a remote part of the anterior-temporal (AT) network and primarily shares connectivity with the sensory, lateral portions of the entorhinal cortex (EC) that do not contain grid cells – with the exception of its most medial portions (Henssen et al., 2016). Consistent with OFC‘s affiliation with the AT-network, Bongioanni et al. (2021) observed that the OFC exhibited repetition suppression for repeated choice identities, but not for latent values appearing within different choice identities. This suggests that the OFC primarily engages in direct choice-outcome associations, relying on prior experience with specific choices, as opposed to extracting abstracted value from an internal model. Conversely, the vmPFC exhibited heightened activity during trials requiring the latter, implying that the OFC may represent model-free associations specific to familiar choices, while the vmPFC encodes model-based and grid-coded representations for novel choices. Nonetheless, research has demonstrated the OFC's involvement in model-based learning, as evidenced by its reflection of model-based prediction errors (Daw et al., 2008; O'Doherty et al., 2003) and its role in decision-making processes that incorporate transitive inference from experience (Padoa-Schioppa & Assad, 2008). Moreover, the distinct representation of value signals for chosen and unchosen options within the OFC's neural populations, independent of sensory modality, stands as one of the most significant discoveries in recent neural decision-making research (Padoa-Schioppa & Assad, 2006). Consequently, the central role of the OFC in the decision-making process is undeniable, irrespective of its involvement in grid-coded representations. It is also essential to acknowledge the heterogeneity of the OFC, with substantial network connectivity variations

between its lateral and medial portions. The medial parts are associated with the default mode network (DMN), similar to the vmPFC, suggesting functional overlap between these regions (Henssen et al., 2016). As a result, differentiating these regions within decision-making tasks remains an ongoing challenge that warrants further investigation.

While the presence of grid code in novel decisions is a critical aspect to consider, it is equally vital to examine its interaction with decision-making hubs in prefrontal regions for a more thorough understanding of the neural foundations of decision-making. Given the intricacies and potential interplay between grid cells and prefrontal regions in decision-making, it is essential to elucidate their respective roles and contributions. Consequently, our study aims to further explore the role of grid cells in novel decision-making processes while analyzing familiarity- and novelty-based influences on decision related activations in prefrontal regions.

Hypotheses

Our study is anchored in the overarching hypothesis that grid cells play a critical role in novel decision-making processes, as participants mentally navigate spatial representations of value to compare new reward options. We specifically hypothesize that neural activity in the posterior medial entorhinal cortex (pmEC) is hexadirectionally modulated by the inferred trajectories derived from a 2D value representation of decision stimuli. Our hypothesis is informed by the understanding that grid cell activity in pmEC may not only be crucial for spatial processing and navigation, but also might reflect the brain's capacity to navigate abstract spatial representations to accommodate complex and novel decisions. We have chosen the posterior medial entorhinal cortex (pmEC) as our region of interest (ROI) as existing studies, such as Park

et al. (2021) and Bongioanni et al. (2021), have mainly concentrated on the ventromedial prefrontal cortex (vmPFC) in their primary grid analysis. Consequently, current evidence for entorhinal grid code in novel decision is solely based on whole-brain effects (largely uncorrected for multiple comparisons), which may not provide a comprehensive or reliable understanding of its specific role. We aim to close this gap by employing a more targeted analysis to this specific region. Furthermore, we propose that this mechanism operates exclusively during novel decision-making processes, where model-based knowledge of action-outcome relationships and generalization are vitally important. If supported, these findings would have significant implications for our understanding of the neural mechanisms underlying decision-making and the domain-generality currently merely supposed for entorhinal grid cells.

In addition to our central hypothesis, we propose related hypotheses concerning prefrontal involvement during the value representation process. First, we expect that the decision phase reveals prominent activity in the orbitofrontal cortex (OFC) across both familiar and novel conditions, as it is known to be crucially involved in decision-making and has been implicated in both model-free and model-based investigations of decision behavior. Therefore, we expect it to be active when participants are comparing reward options, irrespective of whether a decision is familiar and habitual or novel and goal directed.

Additionally, we propose that the decision phase will exhibit significant differences between familiar and novel decisions in ventromedial prefrontal cortex (vmPFC) activity, as this region has been particularly associated with grid-coded representations of novel decisions. Given the involvement of the vmPFC in value-based decision-making and information integration during

decision-making processes, we expect more distinct activation patterns when participants engage in decision-making involving novel stimuli as opposed to familiar ones. This should demonstrate the heightened reliance on inference and generalization in novel decision-making situations.

Methods

Task and Procedure

The present study implemented a computerized binary choice task over three days, requiring participants to select visual stimuli to obtain rewards in the form of points. Each stimulus was characterized by two visual features: color and orientation, which corresponded to reward magnitude and reward probability, respectively. This framework necessitated participants to integrate reward-indicating features for accurate value comparison and theoretically allowed for a comprehensive representation of the value structure through a 2D-feature space (see Figure 1), as was crucial to our hypothesis. The experimental design and task used in this study were based on a similar approach employed by Bongioanni et al. (2021).

Figure 1

Feature Space and Stimuli Set

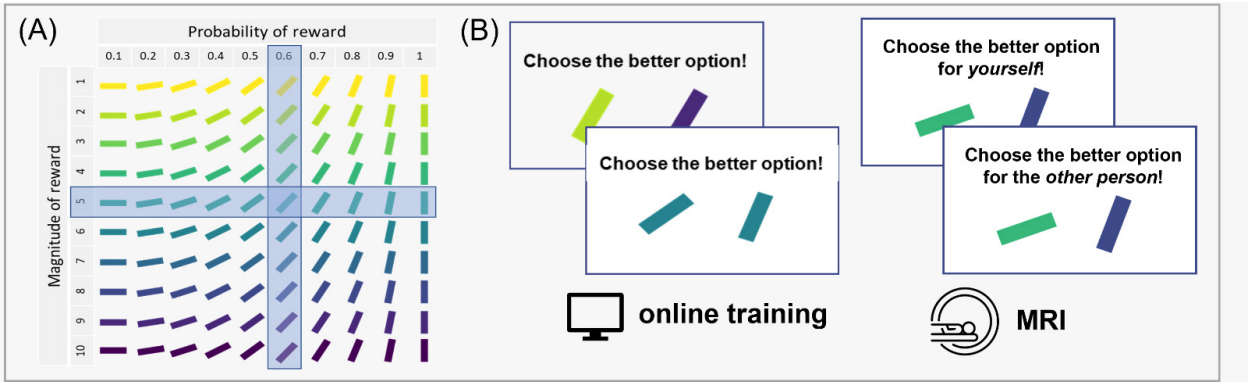

Note. (A) the stimulus space, spanned by vertical axis of reward magnitude (expressed in color variation) and horizontal axis of reward probability (expressed in angular orientation). Familiar choices from training are highlighted in blue. Crucially, participants never saw this 2D-representation of the stimuli space, only successions of binary choices illustrated in B. (B) left side, trails from online training allowing variation in only one of the two value dimensions, right side displays trials from the experimental task during MRI, also allowing for simultaneous variation of both dimensions, thereby generating novel decisions.

Training Phase

Over the first two days, participants underwent training sessions to become familiar with the two dimensions of the stimuli: reward magnitude (color gradient) and reward probability (orientation). Within each training set, stimuli were separated such that variation occurred along only one dimension at a time, while the other remained constant.

Set 1 involved stimuli with varying reward magnitudes indicated by different colors, while maintaining a constant shape orientation (45°) and corresponding reward probability (60%). In Set 2, stimuli varied in reward probability, represented by differing shape orientations, while keeping the color constant (corresponding to a reward magnitude of 5 points). Each set was administered once daily for approximately 30 minutes, totaling two hours of training across the two days. In bot training and the main experimental task, decision responses were collected employing a four-level rating scale, in which participants indicated their preference between

the left or right option while concurrently providing a confidence rating associated with their decision. This method facilitated a comprehensive analysis of the decision-making process by capturing both the selected choice and the degree of certainty expressed by the participants regarding their decision. The inclusion of the confidence measure served to enrich the behavioral analysis.

Main Experimental Task

On the third day, participants were invited to an MRI scanner to perform the main experimental task. During this task, the stimuli simultaneously varied along both dimensions, generating entirely novel feature combinations that participants had no prior experience with. In order to successfully perform on these novel trials, participants had to generalize their experience from training to adequately perform a value comparison for decision making. As such, this task was likely to engage neural substrates of transitive inference during novel choices. This main task was divided into three runs due to the need for recalibration of the MRI and breaks for participants to minimize fatigue. An example of trial progression can be observed in Figure 2. Given that the task took 58 minutes in total, participants were promised an additional 5 Euro bonus for good task performance to maintain their engagement and motivation throughout the task. However, all participants received the bonus regardless of their actual performance, as its primary purpose was to promote task engagement.

After completing the decision-making task, participants were exposed to the stimuli once again, but this time in a different manner. Instead of making decisions between options, the stimuli were presented sequentially, with option B being displayed after option A. This procedure aimed to contrast potential grid-like codes associated with active decision-making against more

passive representations of the underlying feature space. Furthermore, the comparison served to investigate neural representations of decision-making and stimulus identity coding, as described in Bongioanni et al. (2021). However, the analysis of the sequential task falls outside the scope of this master's thesis, therefore relevant literature, randomization, task specification and analysis are not discussed in the subsequent sections.

In the same vein, it is important to mention that an additional condition, specifically a social one, was incorporated in the experiment, although it was not aimed for inclusion in the present thesis. However, it is beneficial to recognize that certain decision trials produced points not for the participants but for a confederate. As a result, all trials were categorized into self-related and other-related decisions, which were displayed in a sequence of 5 trials per block.

Figure 2

Trial Progression during Main Experimental Task

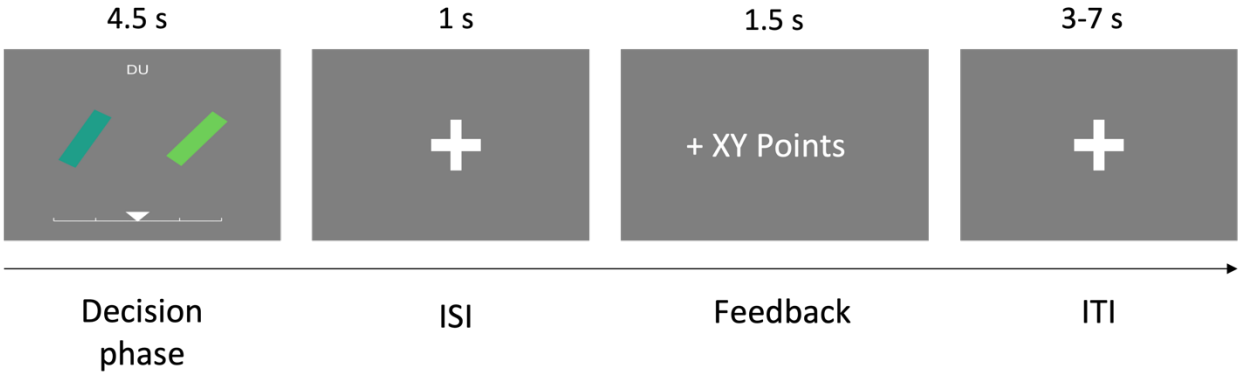

Note. The illustration presented represents a trial from the experimental task on the third day, conducted during MRI scanning.

Power analysis

While most studies examining grid cell representations have primarily focused on (mental) navigation, the reported effects can still serve as a foundation for power estimations, as they characterize the general detection of hexadirectional modulation in neural populations using fMRI. Consequently, our sample size calculations were based on fMRI studies that investigated grid cell representations during self-related (mental) navigation (pooled effect size, d=0.49) (Doeller et al., 2010; Bellmund et al., 2016; Horner et al., 2016). Given this medium-sized effect, we expected to require 35 participants to detect grid cell representations during the experimental task with a power of 80%. Similarly, studies investigating grid codes in abstract, cognitive spaces have employed similar sample sizes. For instance, Park et al. (2021) utilized 25 participants, while Constantinescu et al. (2017) involved 28 participants in their research. However, as the social conditions of our study were exploratory and have not been previously examined, we proposed increasing the participant count to 60 in study design. Regrettably, due to a late discovery of issues with our randomization procedure (see randomization section), we were forced to halt participant recruitment after enrolling only seven individuals. This small group constitutes the entire sample analyzed within this thesis. As a consequence, all subsequent analyses were substantially underpowered. It is hence important to exercise caution when interpreting the results of this study, given the limited sample size and its potential influence on the robustness of the statistical findings.

Participants

Seven healthy volunteers (3 females, 4 males) were recruited from the community and from the University of Vienna. Participants ranged in age from 20 to 25 years (M = 22). All

participants had no history of neurological or psychiatric disorders. Additional exclusion criteria included pregnancy, personal characteristics that made them ineligible for MRI scanning, such as having non-removable metallic objects in the body, active implants, surgical implants, metallic objects in the body, hearing aids, metallic tattoos or claustrophobia. All participants provided written informed consent and the study protocol was approved by the review board of the Ethics Commission at the University of Vienna. Participants were compensated for their time and effort in the study. They had the option to receive either course credit or a payment of 10 Euros per hour, depending on their preference and eligibility.

Stimuli

We used a modified version of the training and experimental task from Bongioanni et al. (2021) more suitable for human subjects. The original task expressed the reward probability dimension in terms of number of dots displayed. To prevent participants from relying solely on dot counting to infer magnitude as the relationship was linear, we used stimuli from Chau et al. (2014) that varied in angular orientation instead. In regard to the reward magnitude dimension, we ensured color-blind friendliness of our stimuli by employing a perceptually uniform color map, Viridis (Garnier et al., 2021). The 2D feature space was discretized into ten levels per dimension, thus generating a total of 100 feature combinations, and an equal number of distinct stimuli (see Fig. 1).

Pilot

A pilot study was conducted with a separate group of participants (n = 13) prior to the main experiment to ensure the validity of the experimental design and determine the amount of

training required for learning the task. The pilot study consisted of the trainings from the main study and an online version of the experimental task. After data collection from seven participants, preliminary analysis revealed that overall accuracy, measured as the relative number of decisions preferring the choice of higher value, fell below the predetermined criterion for successful learning after training (< 90%), indicating a low level of task comprehension. Also, the increase in accuracy between training sessions did not suggest that participants where actively learning. Consequently, additional measures were adopted, including new instructions and an introduction task. The introduction task consisted of a simplified version of the training that allowed participants to become familiar with its requirements. The additional measures successfully improved task comprehension, as evidenced by subsequent sampling results that demonstrated satisfactory mean accuracy (magnitude training: M = 89%, probability training: M = 91%). Regarding the validity of the experimental design, we observed comparable accuracies between familiar and novel conditions on the third day, thereby providing empirical support for participants' ability to successfully infer the value of unseen decisions within our task. As such, the experimental task was deemed effective in promoting generalization and inference of values in novel decisions. This sufficed as proof of concept prior to our main experiment. Additional results can be found in the appendix (Fig. 14).

Randomisation

In the present study, 84 binary choice trials were generated for each run and subject. The trial distribution for the present study was designed to ensure a balanced representation of both

familiar and novel decisions. Specifically, half of the trials were assigned to the familiar decision condition, the other half were assigned to the novel decision condition. Additionally, as the study was performed in collaboration with another thesis investigating self- and other-related decision-making, a social condition was balanced across trials to include both self- and other-related decisions.

Furthermore, in order to prevent confounds, a multitude of subsidiary aspects had to be considered. All trials could take on one out of three relations to our two-dimensional space. They could either be consistent (one option is higher in magnitude and probability), inconsistent (one option is higher in magnitude but lower in probability and vice versa) or lastly 1-dimensional (one option is higher in one dimension but equal in the other). This dimensionality determines the degree of integration needed for adequate value representation and was therefore crucial to be balanced across conditions. Furthermore, across all conditions, the average expected value sum (left value plus right value) was matched as differences in the overall value could have distorted signals (Bongioanni et al., 2021). Expected value difference (left value minus right value) was matched in the same manner across all conditions, except in dimensionality conditions, as these naturally differ in value difference. In preparation for latter grid analysis, it was ensured that trials on aggregate produced trajectories of roughly equal length in all different directions through stimuli space, as imbalances can bias estimated grid orientations in later analysis (i.e grid orientations may be estimated skewed towards unexplored directions). We hence applied a 6-fold symmetrical model which divided the 360° space into 6 directional bins with 10° angular resolution (as used in Doeller et al., 2010, see Fig. 3), and sampled the total distance of trajectories within these bins evenly. Trials were then

generated so that differences in distance “walked” across the directional bins did not differ significantly on aggregate. Additionally, for the purpose of separating self- and other-directed representations of value, all stimuli were assigned onto social conditions to shut out potential spill-over effects. This allocation was performed randomly while ensuring equal value distributions in both conditions. After having generated a balanced trial sequence that met all the above criteria a second step randomised the sequence for each participant and run. Blocked social conditions and limited direct repetitions regarding dimensionality and familiarity conditions characterised this step as a pseudo-randomization. However, within this two-step process of balancing and randomisation, one balanced sequence was used for multiple subjects (instead for one for each subject), adding observations to small mean differences and inflating their significance-level. Due to this issue, data collection and sampling were preliminary halted, and all subsequent analyses was performed on existing sample. Incidentally and fortunately, only the balance of social conditions was significantly affected. However, had we continued data collection using the flawed trial sequences, conditions relevant to the current thesis would have become affected as well.

Figure 3

Directional Bins for Balancing

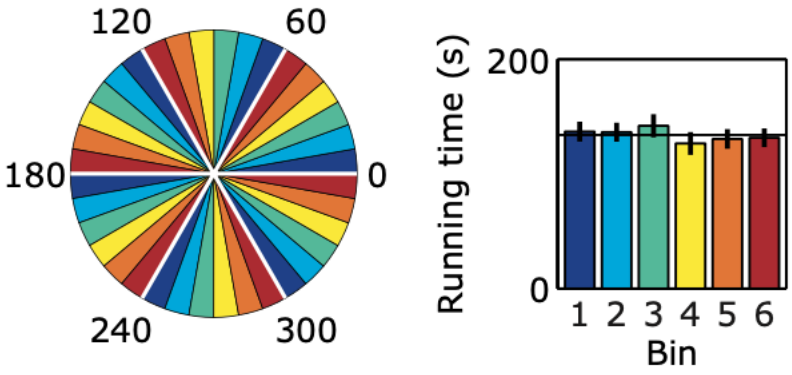

Note. Ilustration sourced from Doeller et al., 2010. By employing a systematic angle allocation, we ensured balanced trajectory lengths across bins, effectively preventing biases in subsequent analyses of grid orientations.

Imaging Data Acquisition

Functional and structural MRI data were acquired on a 3T MRI scanner (Siemens skyra) using a 32-channel head coil. Functional images were collected with a T2*-weighted EPI sequence utilizing multiband scanning to enable faster acquisition (TR = 1000ms, TE = 35.20ms, flip angle = 60°, FOV = 213mm, measurements = 1200, slice number = 66, voxel size = 2x2x2mm). A high-resolution T1-weighted structural image was also acquired for each participant (TR = 2300ms, TE = 2.43ms, flip angle = 8°, FOV = 240 mm, slice number = 208, voxel size = 0.8x0.8x0.8mm), as well as a T2-weighted structural image (TR = 3200 ms, TE = 564 ms, FOV = 256 mm, slice number = 224, voxel size = 0.8x0.8x0.8mm).The use of a mirror attached to the head coil ensured that participants could view the tasks without moving their heads while the placement of the MRI-compatible button box on their chests allowed for response collection without interfering with the image acquisition.

Data Preparation

To preprocess the imaging data, we utilized Nipype version 1.4.2 (Gorgolewski et al., 2011) in conjunction with SPM12 (The FIL Methods Group, 2014) and FSL (Smith et al., 2004) modules. The preprocessing pipeline comprised of several steps, including the conversion of DICOM data into NIFTI format, eliminating dummy scans, correction for slice timing variations and head motion correction using six parameters with the mean volume as a reference. Furthermore, to readily achieve spatial localization and for group-level analyses, we normalized all functional images to the Montreal Neurological Institute (MNI) space through tissue segmentations of structural images. Additionally, we applied spatial smoothing after normalization with an isotropic Gaussian kernel having a full width at half maximum (FWHM) of 5 mm.

To assess the plausibility of our MRI data after the preprocessing procedure, we examined contrasts unrelated to our hypothesis. For instance, we investigated whole-brain activity during feedback for successful decisions (outcomes yielding points) and contrasted it with non-successful decisions (outcomes of zero points). The results revealed positive clusters in the brainstem (x = 4, y = -28, z = -30, cluster mean = 3.617), amygdala (x = -32, y = 0, z = -22, cluster mean= 3.642), and caudate nucleus (x = 14, y = 8, z = 0, cluster mean = 3.55724), suggesting higher involvement during win trails (see Appendix, Fig. 17). These findings align with well-established neural effects of reward processing (O'Doherty et al., 2003), thereby supporting the plausibility of the data prior to main analysis.

Behavioral Analysis

Behavioral analyses were conducted using the R Version 4.1.2 to confirm the presence of learning during training and adequate comprehension of the task during imaging. Descriptive

statistics were generated and the results were plotted to identify similar patterns as observed in the pilot study. Descriptive statistics were also examined for plausibility checks and identification of irregularities, such as outlier detection. No response trials were omitted in all analysis.

Moreover, inferential tests were used to investigate the effect of familiarity on various performance measures, such as accuracy, confidence, reaction time (RT), and inconclusiveness (the number of changes of the preferred choice within the decision time-frame). Due to our small sample size, we employed the Wilcoxon rank sum test, which is a robust non-parametric alternative to the t-test, to assess the differences in measures between the two conditions. We adopted a significance level of $p < 0.05$ throughout the behavioural analyses.

Mass Univariate fMRI Analysis

The first-level analysis of the neuroimaging data was carried out using nilearn and spm12 software within a Nipype environment. A general linear model (GLM) was employed to perform event-related fMRI analyses for each individual subject. The first-level model parameters included a repetition time (TR) of 1 second, a slice time reference of 0.445, and an autoregressive noise model of order 1 (AR1), which accounts for temporal autocorrelation in the fMRI time series. The hemodynamic response function (HRF) followed the SPM standard, and no drift model was incorporated. A high-pass filter with a cutoff at 1/128 Hz was applied to mitigate low-frequency noise. Additionally, six motion parameters were included as regressors in the GLM to account for potential confounding effects of head motion. This streamlined model facilitated the identification of brain regions with significant correlations to the experimental task and conditions within each subject.

To test our hypotheses, we applied two main contrasts to investigate the differential neural circuits underlying familiarity-based decision making in whole-brain activity. Specifically, the first contrast aggregated all data from the decision phase, including both familiar and novel trials, and compared it to the baseline activation where we anticipated significant clusters in the medial prefrontal regions, specifically the OFC.

In the second contrast, we exploited the activation during the decision phase to identify maximal differential activation between familiar and novel trials (familiar minus novel trials), which was expected to be present in the vmPFC.

The second-level analysis was performed using nilearn's 'SSecondLevelModel' function. A design matrix consisting only of an intercept term was created for the group-level analysis to capture the grand mean across subjects. The purpose of this uncover consistent group-level effects by accounting for variability across individual subject-level contrasts.

To maintain experimental validity, we carefully examined data derived exclusively from self-directed decisions, systematically excluding 50% of both familiar and novel trials. This was employed to minimize influencing factors arising from the social condition. Furthermore, we applied the conservative family-wise error correction to decrease the likelihood of type-1 errors, ensuring a more robust analysis. This approach enabled us to examine the neural correlates of our hypotheses in a more controlled and statistically rigorous manner. However, due to the small sample size and conesquentially underpowered tests, we also conducted a second exploratory analysis that incorporated more trials by aggregating across social conditions, thus providing twice the amount of trials for analysis. In this analysis, we also loosened constraints on type I error control by applying False Discovery Rate (FDR) correction

instead. By utilizing more conservative statistical correction methods in our primary analysis and more liberal approaches in our exploratory analysis, while simultaneously loosening validity criteria for experimental trials, we aimed to balance scientific rigor with the limitations imposed by our small sample size. To accurately localize and label the brain regions exhibiting significant activation with respect to our contrast, we utilized the Harvard-Oxford atlas, provided by the Harvard Center for Morphometric Analysis.

Grid Analysis

We used the GRIDCAT toolbox (Stangl et al., 2017) in our analysis to assess the presence of metric properties of grid cells in our fMRI data. The analysis was performed using MATLAB R2020a and SPM12. In the first step, similar to conventional GLM analysis, we characterized the events of interest in our time series, specifically the decision phases of self-related, novel trials. Furthermore, each timestamp or decision phase was denoted with its corresponding trajectory in value space, characterized as an angle relative to a predefined, yet arbitrary reference point (0°) (see Figure 4, A). In a next step, GRIDCAT requires partitioning of the data to perform parameter estimation (GLM1) and model testing (GLM2) independently (see below for detials of the GLMs). Such a two-step process is good practice for complex model fits because it minimizes the risk of overfitting, allowing for a more accurate assessment of the model's performance on unseen data. As grid analysis was conducted on the basis of individual runs, we partitioned our data within each run for this step. Despite this, the following results section exclusively reports on parameters averaged across runs, as we would provide a more reliable representation of the underlying grid cell patterns. Notably, we used the same normalized and

smoothed images as in previous whole-brain analysis. Furthermore, we motion parameters from preprocessing specific to our ROI were added to the analysis. More intricate parameter settings within the GRIDCAT-toolbox were kept at default (masking threshold, micro-time resolution etc.).

In the method employed for the estimation data (GLM1), decision angles serve as the basis for generating two parametric regressors , specifically sin(α * 6) and cos(α * 6), with α symbolizing the grid event angle. The multiplication factor 6 in this operation translates the grid event angle into 60° periodicity, reflecting the hexadirectionality known from the firing fields of grid cell. By incorporating these regressors into the GLM, voxels exhibiting significant signal modulation in accordance with the proposed phase shifts would yield high beta weight estimates, indicating good model fit. Upon computing voxel-wise grid orientations, we conducted a subsequent analysis (GLM2) in which we averaged grid orientations across voxels within the pmEC-mask and aligned decision angles relative to this reference point. As previously noted, we chose the pmEC as our ROI due to its high concentration of grid cells and its unique connectivity profile with the vmPFC (Ranganath & Ritchey, 2012). In order to focus our analysis on this region, we utilized an anatomical mask targeting the posteromedial entorhinal cortex (pmEC) within the MNI standard space. While it has been suggested that analyzing data in subjects' native space may be beneficial for small sample sizes with potentially weak signals (Stangl et al., 2017), using normalized data in standard space was chosen for practical reasons, despite the potential for spatial distortions and interpolation errors. To calculate the ROI-specific mean grid orientation, the beta estimates (β1 and β2) linked with the two parametric regressors from GLM1 were averaged for all voxels in pmEC. We then took the arctangent of their ratio, which normalized

the value within the range of angles. Finally, this angle was divided by six due to the redundancy caused by the symmetry, providing us with the unique orientation of the mean grid's symmetry. Subsequently, decision angles were defined based on their alignment with the six-fold symmetrical model centered around the mean grid orientation. It was expected that greater neural modulation would be observed for higher degrees of alignment. This modulation is anticipated due to the effect of fMRI adaptation, which is a reduction in signal when a representation is activated repeatedly compared to when it was previously inactive. During runs aligned with the grid, fewer grid cells are anticipated to fire, but they do so at a higher rate. In contrast, during misaligned runs, more grid cells are active but at a lower rate (see Doeller et al., 2010 for a more detailed explanation). As a result, trajectories that are completely aligned with the mean grid would more reliably and repeatedly stimulate the same grid cells, leading to greater neural modulation.

As such, parametric regressors for GLM2 were calculated by determining the alignment between each decision angle (α) and the mean grid orientation using the function cos[6*(α – mean grid orientation)]. Resulting values ranged from -1 to 1, with positive values indicating greater degree of alignment (See Figure 4, C) Beta estimates derived from GLM2 quantified the degree of neural modulation exerted by the hexagonal symmetry model, centred around participant-specific mean grid orientations. These so called “grid magnitudes” functioned as the primary metric for hypothesis evaluation.

We assessed whether grid magnitudes were significantly greater than zero, implying a suitable model fit and substantiating the presence of grid-like modulation in neural activity. To assess the statistical significance of grid magnitudes, we employed the Wilcoxon Signed-Rank Test, a

non-parametric alternative to the one-sample t-test, which enabled a robust examination of limited sampled parameters. Additionally, we applied same procedure to models proposing alternative sinusoidal patterns, such as 5-fold and 7-fold rotational symmetries, to ensure that effects were specific to patterns known of grid cells and not merely the result of overfitted statistics.

Following the completion of both GLM's, additional model parameters need to be examined before interpreting the results. One critical aspect considered was the stability of grid orientation, as it can significantly impact the estimation of grid orientations and subsequent grid magnitudes. Therefore, we carefully investigated grid-orientation stability in terms of both between-voxel coherence (spatial stability of grid orientation) and within-voxel consistency (temporal stability of grid orientation). Temporal stability was assessed by comparing voxel-wise orientations in the first run to the last run. If the discrepancy in orientation estimates between the timepoints did not exceed a tolerance threshold of 15°, the orientation was considered temporally stable for that voxel. The final measure for temporal stability was then represented as the percentage of stable voxels within the ROI. Spatial stability, or coherence, was computed using Rayleigh's test for non-uniformity in circular data. Its z-values indicate significant clustering of grid orientations among voxels within a given ROI and is thus used to measure spatial stability. This approach allowed for a comprehensive examination of the grid-orientation stability across time and space, providing a solid basis for model evaluation.

Figure 4

Illustration of Trial Specific Decision Angle

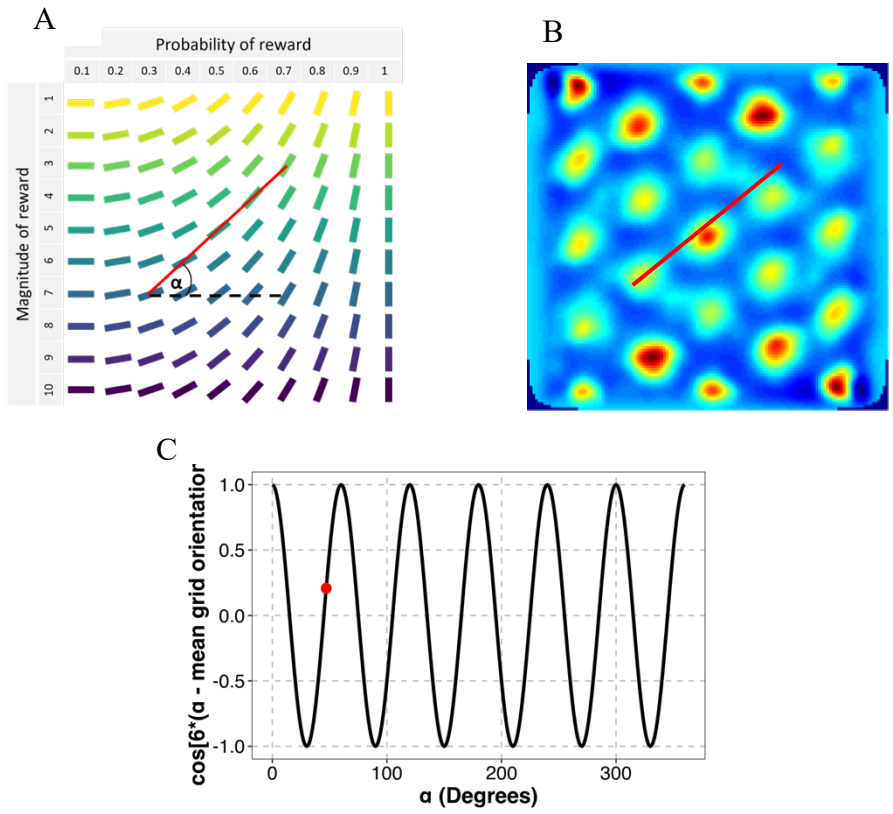

Note. (A) The trajectory (red line) linking two choices is depicted in 2D stimulus space. This representation of our binary-choice task characterizes each with a unique decision angle, α, relative to an arbitrary reference point at 0° (dotted line). (B) Grid cell image sourced from Doeller et al. (2010), exhibiting a hypothetical alignment/misalignment of the trajectory with the grid cell orientation, which influences their activity. (C) The regressor in GLM2 parametrically represents the alignment of α the with the average grid-orientation. Higher values indicate a greater degree of alignment.

Results

Behavioral results

Our analysis demonstrates an accuracy rate of approximately 80% throughout both training and testing phases (see Fig. 4A), which is what we expected from earlier studies by Bongioanni et al. (2021), Park et al. (2021a) and Constantinescu et al. (2016). The similar performance observed between familiar and novel conditions (see Fig. 5A) supports the participants application of zero-shot learning. Participants were capable of accurately inferring the values of choice options for novel stimuli without prior exposure, suggesting that an internal model of value structure within the task facilitated the generalization of learning from familiar to novel situations. However, inferential statistical analyses did not reveal significant differences in any dependent variables between familiarity conditions (all p-values > 0.05) (see Appendix, Table 6). Consequently, our data does not indicate a differentiation of decision-making processes between familiarity conditions at behavioral level.

Contrary to our assumptions, confidence ratings associated with each choice did not substantially increase during training and displayed highly similar results regarding familiarity conditions (see Fig. 5B).

Figure 5

Accuracy and Confidence Across Sessions and Tasks

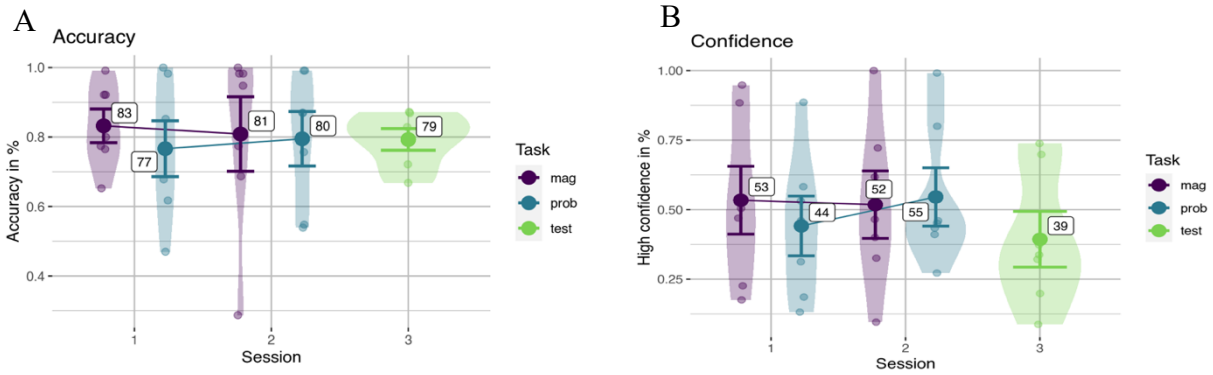

Note. Error bars represent 95% confidence intervals
Specific note. (A) high accuracy in first training session in conjunction with low increase to the second session indicates that most of the learning occurred within the first session.
Specific note. (B) Confidence ratings close to identical between familiarity conditions.

Mean accuracy scores across dimensionality conditions reflected the expected difficulties arising from the varying levels of value-integration necessitated in these trials (see Fig. 6). Furthermore, a biserial correlation analysis revealed a statistically significant positive correlation between value difference and correct responses ($r = 0.215$, $p < 0.05$). A significant positive correlation of 0.22 ($t = 9.4494$, $df = 1750$, $p < 2.2e\text{-}16$) was also observed between value difference and confidence ratings. While these positive correlations are consistent with our expectations, the rather moderate effect sizes raise concerns about the validity of our task. The limited influence of value-difference on actual decision-making I suggests that the neural representation of value-difference may not have played a substantial role in driving dIbehavior.

Figure 6

Accuracy by Dimensionality Conditions

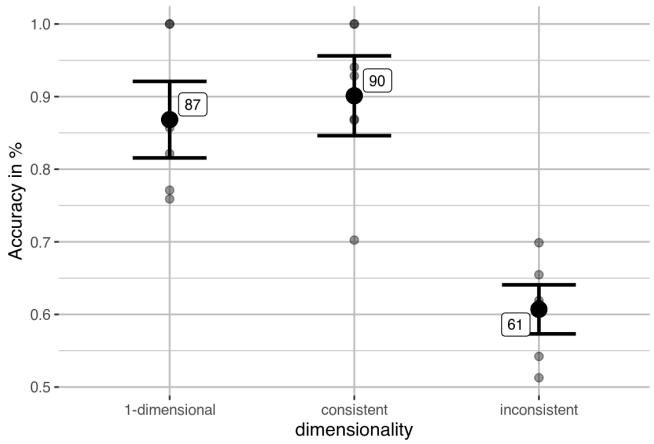

Note. Error bars represent 95% confidence intervals. Decision-making trials encompassed three conditions: (1) one-dimensional, in which choices differ based on a single feature, akin to the training phase; (2) consistent, where choices exhibit variation across both features, and the superior option demonstrates higher values in both dimensions; and (3) inconsistent, where choices display variation in both dimensions, but each option possesses a higher value in one dimension respectively.

The observation of equal performance between familiar and novel conditions (see Fig. 6) provides evidence for zero-shot learning, as demonstrated by the accurate inference of choice option values for novel stimuli. This result indicates that participants were capable of generalizing their learning from known decisions to new, previously unencountered decisions without any explicit training or exposure to these novel choices. The inferential statistics between familiarity conditions revealed no significant differences in regard to any of our behavioral measures (all p-values > 0.05). (See Appendix, Table 6).

Figure 7

Accuracy and Confidence by Familiarity Conditions

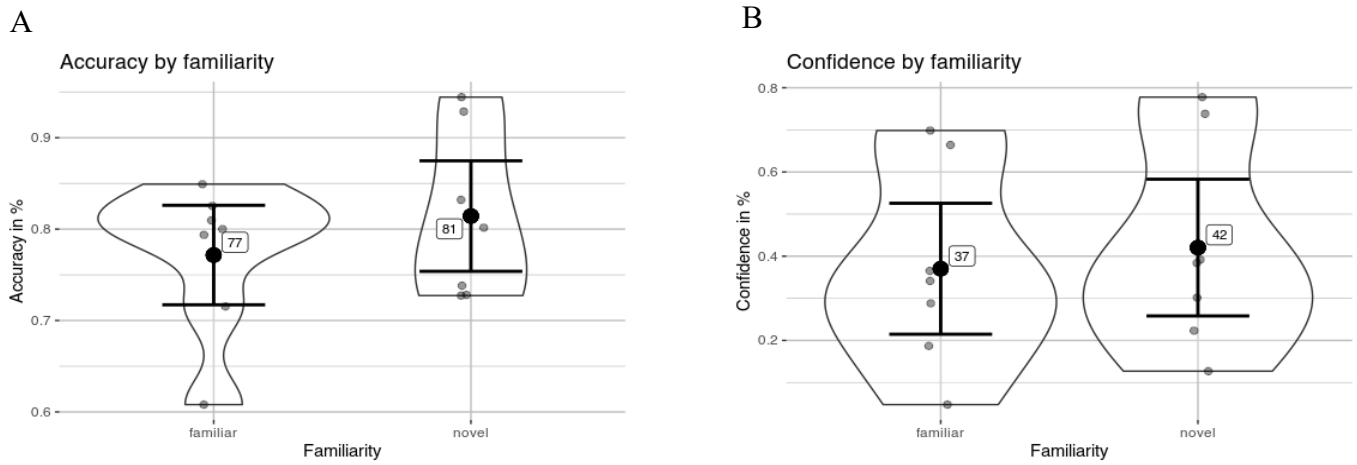

Note. Error bars represent 95% confidence intervals.
Specific note (A) no significant differences in accuracy, although slightly higher average during novel trials.
Specific note (B) Confidence ratings close to identical between familiarity conditions.

Mass Univariate fMRI Results

Main Analysis

By focusing exclusively on self-related decision trials and applying a Bonferroni correction with an alpha of $p < .001$ and a minimum cluster extent threshold of 10 voxels, we were unable to identify significant clusters in our analysis. This was the case for both whole-brain contrasts examined: (1) decision phase > baseline, and (2) familiar > novel during the decision phase. Consequently, two hypotheses were rejected: one proposing a positive main cluster in the OFC during the decision-making phase, and another suggesting differential engagement of the vmPFC based on the familiarity conditions of decisions. Aside from true absence of effect, this outcome could be attributed to the stringent nature of the statistical methods employed, as it may have to strongly prioritized the minimization of Type I errors, given our small sample. This

might have resulted in the exclusion of subtle, yet meaningful effects related to neural activity during the decision phase.

Explorative Analysis

After incorporating all decision trials, implementing a false positive rate (FPR) correction with an alpha level set at 0.001 and a minimum cluster extent of 10 voxels, the results of our analysis indicate that there were 23 statistically significant clusters (see Table 1, see Fig. 8). Contrary to our initial hypothesis, the OFC and large portions of the mPFC were found to be part of significant cluster with negative z-scores. This unexpected result indicates suppressed activation during the decision phase, rather than the anticipated increase in activation.

Table 1

Decision phase (Decision phase > Baseline), 25 significant clusters

Brain region	MNI coordinates			z-value	Cluster mean	Cluster size
	x	y	z			
R mOFC	40	18	-6	-3.911	-3.502	120
L ACC	3	30	-8	-4.688	3.952	88
L Frontal Gyrus	-20	28	40	-4.31227	-3.66928	336
L Precuneus	-2	-52	18	-3.743	-3.464	144

Note. This table reports the local maximum within clusters and corresponding MNI coordinates of peak activation voxels. Effects were considered significant using a cluster-defining threshold of p > .001 and a cluster size > 10 voxels. False positive rate (FPR) correction was performed at cluster-level and used to adjust for multiple comparisons.

Figure 8
Decision phase > Baseline

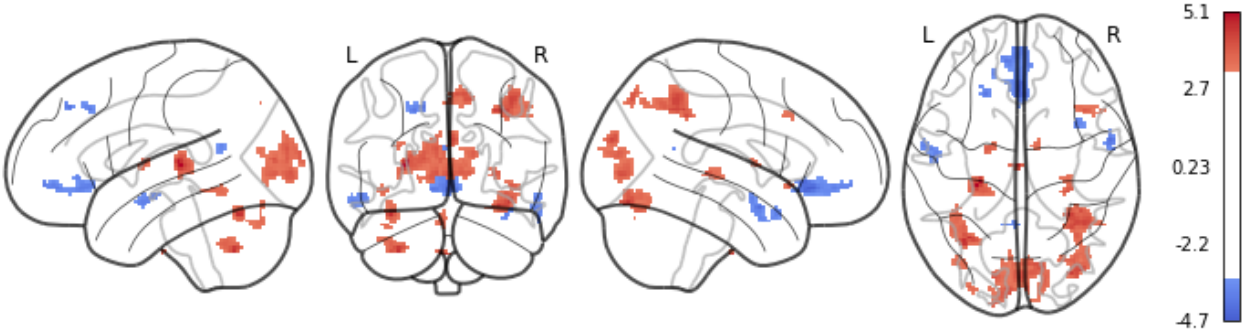

Note. Results were shown at p < 0.001, FPR corrected, and a minimum cluster size of 10 voxels.

In examining the differential neural signals involved in familiar and novel decision-making tasks, using a liberal threshold (false-positive rate correction, p < .001) and the full dataset, only two significant clusters were identified (see Table 2, see Fig. 9) This finding contradicts the initial hypothesis suggesting a role for the vmPFC in this context. Instead, an entirely different set of regions responded to the contrast between familiar and novel decision-making.

The right parahippocampal cortex (PHC) displayed significantly greater activation in response to novel trials compared to familiar trials. Furthermore, a cluster encompassing both occipital (cuneus) and parietal (precuneus) cortices demonstrated significantly increased activation during novel trials compared to familiar trials. These results suggest that these clusters are specifically engaged in processing novel information during decision phase. The significant PHC cluster was a noteworthy prerequisite finding for subsequent analysis of grid codes in the pmEC, as it indicated significant activity within its immediate vicinity.

Table 2

Decision Phase (Familiar > Novel), 2 Significant Clusters

Brain region	MNI coordinates			z-value	Cluster mean	Cluster size
	x	y	z			
R Parahip	20	-26	-12	-3.847	-3.432	96
R Precuneus	24	-68	28	-4.416	-3.669	400

Note. This table reports the local maximum within clusters and corresponding MNI coordinates of peak activation voxels. Effects were considered significant using a cluster-defining threshold of p > .001 and a cluster size > 10 voxels. False positive rate (FPR) correction was performed at cluster-level and used to adjust for multiple comparisons.

Figure 9

Novel > Familiar

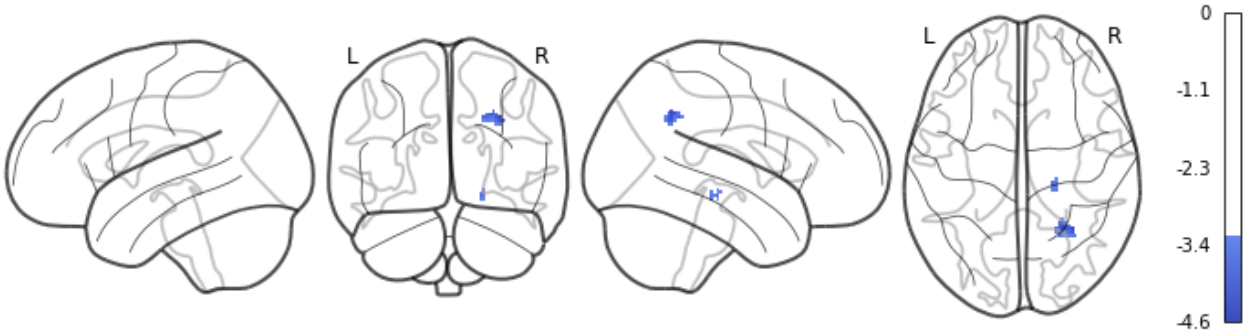

Note. Results were shown at p < .001, FPR corrected, and a minimum cluster size of 10 voxels.

Grid Results

Our results did not provide evidence for the presence of a grid cell activity in the pmEC during novel trials. The grid magnitudes, estimated for a six-fold symmetry, were not significantly

different from zero across subjects (see Fig. 10), thus refuting our hypothesis that decision angles from abstract value space would exert hexadirectional modulation of neural activity. The control analysis showed that the 6-fold symmetry was indistinguishable from other rotational symmetries (see Appendix, Fig. 19), further supporting our conclusion that there was no evidence of grid coding in the pmEC.

Figure 10

Grid Magnitudes for Six-Fold Symmetrical Model

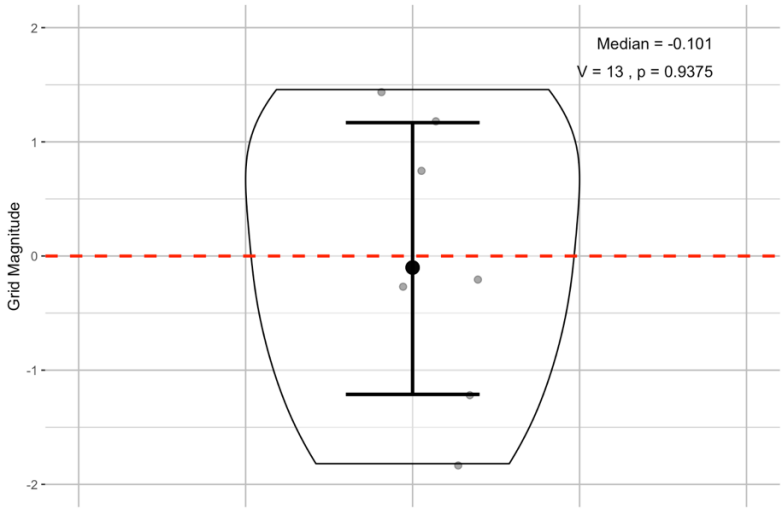

Note. The figure displays grid magnitudes while incorporating results from a Wilcoxon Signed-Rank Test, evaluating whether the parameter estimates for grid magnitudes are significantly greater than zero. The red-dotted line represents the zero threshold. Error bars represent 95% confidence intervals.

The assessment of grid code stability of the 6-fold model yielded ambiguous outcomes. In terms of between-voxel coherence, we observed an average Rayleigh's Z value of 12.92 and a standard deviation of 8.89, indicating variability in the spatial coherence measurement across our sample. However, all participants' Rayleigh's Z values exceeded the critical level, thereby

providing sufficient evidence of spatial stability between voxel. We tested the temporal stability of grid orientation within voxels across multiple runs by calculating the percentage of agreeing grid orientations. To quantify the temporal stability of grid orientations, we examined the consistency between runs 1-3 and computed the average percentage estimate across the comparisons. Our analysis revealed that, on average, 45.57% (SD = 7.38) of all voxels in the pmEC exhibited stable activity patterns across participants. While temporal stability did not display optimal values, they did not introduce systematic error to our grid magnitude estimates (see Fig. 11).

Figure 11

Correlation of Grid Magnitude with Within- and Between Voxel Coherence

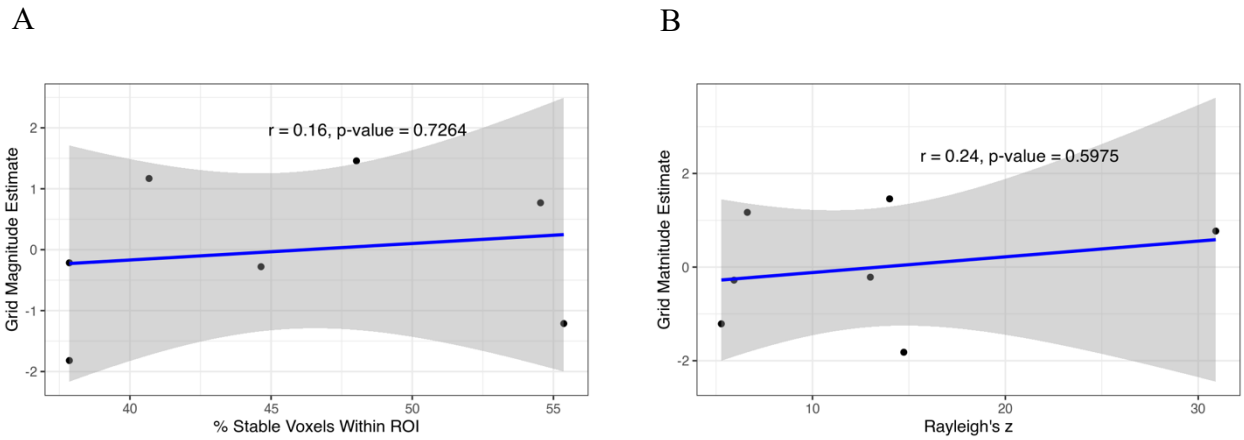

Note. Blue line represents LM-regression line corresponding to the correlation. Shaded area represents error estimates.
Specific Note (A) Weak and non-significant correlation between temporal stability and estimated grid magnitude. Notably, correlations formed on alternative within-voxel stability estimates, comparing temporal stability individually across runs 1-3 revealed similar results.
Specific Note. (B) Weak and non-significant correlation between spatial stability and estimated grid magnitude. Both considered, GLM2 was not likely not influenced by a lack of consistency of measurements from GLM1.

Discussion

In this study, our objective was to investigate the neural underpinnings of novel decision-making processes, specifically focusing on grid cell activity in the pmEC. Furthermore, we hypothesized that there would be differential prefrontal activation based on decision familiarity during the decision phase. However, our results did not provide evidence for grid-like coding of the abstract value space in the pmEC during novel choice evaluation. Additionally, we did not observe differential involvement of the OFC and vmPFC in relation to the familiarity of decisions. However, a more liberal exploratory analysis revealed significant involvement of parahippocampal and precuneus cortex during novel trials compared to familiar trials, suggesting a distinct functional role in making novel decisions. Furthermore, behavioral analysis demonstrated participants' ability to infer novel choice values with accuracy comparable to familiar trials, indicating active inference and suggesting engagement of representations that enable experience generalization to new instances.

Although the small sample size and liberal analysis threshold raise concerns regarding the reliability of these exploratory findings, applying the liberal statistical control to the experimentally conservative selection of valid trials, which comprised only half of the data, generally reproduced the results from the analysis containing the entire dataset, as seen in the appendix (see Fig. 12, Fig. 13). This consistency across separate data subsets helps alleviate some of these concerns and strengthens the validity of the results, as it suggests that the observed effects are less likely to be the result of noise or confounding signals within the data, given that such factors would facilitate random variations. Taking into account this increased

confidence in the exploratory analysis results, we may cautiously interpret the activity within the spatial networks as playing a role in novel decision-making.

Given that both the PHC and precuneus cortex are part of the PM-network and as such commonly associated with abstract relational memory and spatial processing (Ranganath & Ritchey, 2012), our results provide some evidence for the involvement of the spatial navigation system and its novel choice inferences, even in the absence of evidence for the grid-like coding of value information. As such, while we could establish their association to novel choice inference, we could not provide the evidence for the presumable representational format by which they do so, meaning the grid code, which was our main objective. Nonetheless, given that the PHC has been shown to reveal grid code during mental navigation (Doeller et al., 2010) and the precuneus revealing grid code during novel choice inference (Park et al., 2021a), our results are still in line with that grid code may be utilized to organize experiential knowledge for generalization in face of novelty. Furthermore, given that the medial EC primarily connects to the PHC (Nielsen et al., 2019; Ranganath & Ritchey, 2012), any examination of EC grid cell activity within larger cortical networks inherently expects some degree of PHC involvement, irrespective of whether grid coding is investigated for spatial or abstract representations.

Although the precuneus is part of the DMN and typically displays anticorrelated activity during goal-directed tasks, it has been implicated in specific attentional processes and goal-directed behaviors, especially those involving spatial processing and mental imagery (Cavanna & Trimble, 2006). As a component of both the PM-network, responsible for contextual and relational memory, and the self-referential DMN, the precuneus is linked to self-related spatial cognition, such as updating self-position through visual trajectory input (See Cavanna &

Trimble, 2006 for extensive review of multiple lines of evidence) as well as in distance updating during path integration (Chrastil et al., 2015), resembling functions commonly attributed to grid cells in the mEC. Furthermore, recent research has specifically associated the precuneus with learning and memory aspects in spatial navigation and reasoning. Schott et al. (2018) pinpointed the precuneus as a crucial region for forming intricate long-term memory traces of spatial associations. Similarly, Müller et al. (2018), employing transcranial magnetic stimulation to mimic lesions, unveiled the precuneus causal role in preserving and updating object-location associations in space and subsequently incorporating these into sophisticated spatial representations - cognitive maps. It is reasonable to infer that this role of the precuneus in spatial navigation would extend to navigating stimulus association in abstract, cognitive spaces. Given that these exploratory findings align with our initial assumptions about the involvement of spatial networks in representing novel choices, it is somewhat surprising that the associated prefrontal counterpart, the vmPFC, shows no effect whatsoever in the contrast. Apart from attributing this to the most immediate interpretation of a true negative finding or a false negative finding due to underpowered tests, there exists an alternative explanation for the somewhat obscure prefrontal results observed in all our contrasts. However, a clearer understanding of this issue can be obtained by first examining the contrast formed for the analysis of the main effect of the decision phase and its corresponding OFC activity.

During our investigation of the main effect of decision phase on whole-brain activity, covering all social, familiarity and outcome conditions (decision phase compared to baseline), we observed a substantial cluster of negative activation in the MPFC. This outcome contradicted

the anticipated direction of effect, specifically in relation to the OFC (Bongioanni et al., 2021; Constantinescu et al., 2016) but also the vmPFC (Park et al., 2021a). We postulate that this result may be partially attributed to the high level of task engagement and visual demand during the decision phase. The observed suppression of mOFC and vmPFC, both integral parts of the MPFC cluster, may seem unexpected when viewing these regions from the PM-network perspective. However, this outcome can be reconciled by considering their affiliation within the DMN (Raichle et al., 2001). Therefore, it is important not to interpret the large negative cluster solely in terms of decision-making effects, if at all, but instead as a component of the DMN's characteristic task-negative activity pattern. Consequently, task-related suppressions could have obscured or "swamped" more nuanced decision-related influences in the mOFC and vmPFC regions. Notably, while the familiar > novel contrast does not directly compare effects to the baseline, a potential vmPFC's sensitivity to the novelty of decisions may still have been nullified, as the potentially larger task-negativity would unlikely discriminate between these conditions. While speculative, our data does provide some indicators that task-related suppressions may have had a confounding influence.

Firstly, upon examining peak values in the overall negative MPFC cluster, we found positive peaks for the mOFC (x = 40, y = 18, z = -6, peak = 3.910). Despite peak values being subject to noise and random variations, and as such unsuitable for scientific conclusions, these peaks still suggest the existence of counteracting effects within these regions, possibly concealing smaller relevant effects due to nearby confounding, task-negative activations.

Secondly, we can leverage the close relationship between decision-related and feedback-related signals in mOFC (and the broader MPFC area), along with the pronounced differences in

task engagement and visual load during these experimental phases, to gain a general understanding of how task engagement itself may have influenced mOFC activity. When considering the mOFC's involvement in reward processing through frontostriatal and frontolimbic circuits (Daw et al., 2011; Daw et al., 2005) and its role in updating option values based on previous decision outcomes (O'Doherty et al., 2003), we can expect feedback-related activity within the mOFC. Furthermore, Rudebeck and Murray (2013) reviewed studies examining the role of the OFC in decision-making and feedback-processing, finding that OFC neurons encode both expected reward values during decision-making and actual outcomes during feedback-processing. Although the magnitude of signals or effects may vary, their evidence suggests that these signals are correlated and in close proximity, supporting the idea of continuous reward value representation across decision-making and feedback-processing.

Indeed, when examining the main effect of the feedback phase (feedback > baseline), a significant and anatomically more distinct cluster is revealed in the mOFC, which responds with significantly increased activation during the feedback phase (see Appendix, Figure 17). Not only does this cluster much more align to known mOFC function, it also constitutes a more anatomically distinct effect, as the Harvard-Oxford atlas classified the cluster as 100% mOFC. Of course, one could argue that feedback signals are more pronounced in mOFC, as exact effect size estimates are hard to find. Furthermore, one could assume that the smaller and more distinct cluster could be attributed to mere random fluctuations. However, a more plausible explanation is that our feedback phase involved neither significant visual load nor any

requirements for focus and task engagement, thus allowing for better detection of task-positive signals within prefrontal, DMN-associated regions.

An increased sample size may have alleviated these confounding influences during the decision phase by enhancing the detection of subtler patterns in aggregated activity. However, it is crucial not to solely attribute this confound to insufficient analytical power, but rather to consider it as a limitation in our study design. We may hence contemplate solutions that might have enhanced our findings.

For one, implementing a targeted ROI-based analysis could have facilitated a more efficient examination of the relevant clusters. This approach could have involved fitting parametric regressors to time-courses to assess whether variations are influenced by the value difference of choices on a trial-by-trial basis, ideally incorporating both objective and subjective value measures. This might have resulted in more refined and unambiguous findings regarding decision-related activity. Moreover, designing the task to display choice alternatives before and separately from the actual decision phase, when participants make their response, could have aided in distinguishing the value representation in vmPFC from its suppression following visual processing and external attention guidance.

Lastly, rather than comparing the decision phase to resting-state data from inter-trial intervals (ITIs), we could have adopted the approach used by Deny et al. (2012) and compared it to non-mentalizing baseline conditions - an arbitrary yet similar task, likely to exert a comparable influence on DMN regions. This method could provide a more elegant and insightful analysis of the decision-making process.

In regard to our grid analysis, it may be valuable to reassess the analysis using the entire dataset, as data subsets from social conditions appear to show consistent results across multiple analyses. However, when setting aside explanations for our null-result related to power issues and true negatives, we may inquire why we were unable to find grid-coded activations, as previously discovered by Park et al. (2021a) and Bongioanni et al. (2021). A more in-depth examination of the experimental conditions under which they obtained their results could potentially illuminate our inability to replicate their findings.

For example, as mentioned earlier, Bongioanni et al. (2021) did not identify grid code during their actual decision-making task, which served as a blueprint for our task, but rather during a passive viewing task, where stimuli were displayed sequentially without requiring any decisions. The grid code was subsequently revealed by considering the transition from one stimulus to the next as a trajectory through a 2D space delineated by stimulus features. Similarly, Park et al. (2021a) also utilized a sequential task design in which stimuli were displayed in a successive manner prior to the actual decision phase. Notably, this study demonstrated grid-coded representations of abstract, cognitive space during the actual decision-making process.

Numerous reasons could account for the discrepancy between their results and ours, but a salient commonality in the limited demonstrations of grid code in decision-making appears to be the incorporation of sequentiality in their tasks. This is not a trivial aspect, as spatial networks within the hippocampal formation are recognized for sequential coding of events, as evidenced early on by the sequential reactivation of experienced locations within place-cell populations during sleep (Wilson & McNaughton, 1994). This has not only inspired broader

insights into replay and memory consolidation but also characterized hippocampal activations concerning their sensitivity towards sequentiality, inherent to all episodic events. In a more directly related context, Schuckl and Niv (2018) investigated whether experiences from non-spatial decision-making tasks are equally subjected to sequential reactivation and confirmed that latent states of the decision-making task were reactivated in their sequential order in the hippocampus.

Taking the above into account, tasks presenting reward options sequentially rather than simultaneously may more effectively allude to the neural codes observed in hippocampal structures, encompassing trajectory representations within pmEC grid cells. Consequently, further analysis of our sequential viewing data might yield more promising outcomes than the parallel decision task examined in this thesis. However, as previously mentioned in the theoretical background, such findings could be significant for establishing the domain-generality of grid-codes, as they would, for instance, imply their presence in perception and object categorization. Nonetheless, they would remain inconclusive concerning the specific issue of decision making, as they provide no insights into activations during actual choice comparison. As a result, tasks that integrate the element of sequentiality with the requirement of decision-making may prove more advantageous.

An alternative consideration for the grid analysis results involves adopting a different approach in our second General Linear Model (GLM2). Rather than characterizing decision angles parametrically based on their alignment to the six-fold symmetrical model centered around the mean grid orientation, we could discretize the 360° space into multiple bins, each with distinct regressors. Specifically, we could utilize regressors to accommodate the six directional bins,

each with a 10° angular resolution. This partitioning had been implemented during balancing, ensuring that each regressor would receive equal total distance traversed in the abstract value space. These regressors would then define each decision trail as either aligned or misaligned to these models, facilitating subsequent contrasts. The advantage of this method is that it could potentially capture grid-coded events across all decision angles, rather than being limited to those in proximity to the mean grid orientation.

In summary, although our study did not confirm our hypothesis that the pmEC, OFC, and vmPFC have distinct roles in the decision-making process, we recognize the potential of the paradigm used. Increasing the number of participants to reach the intended sample size may still reveal insights and prove the effectiveness of the methos employed. Additionally, the preliminary analyses conducted in this thesis provided early indications of potential flaws in our study design and analytical methods, which could be addressed in ongoing research.

While the issue of domain generality of grid codes may not appear crucial at the moment, it has the potential to prove highly significant in the future. The remarkable impact that grid codes have already had on our understanding of the brain's spatial navigation system underscores their potential to advance our knowledge in a variety of cognitive domains, making it a research area worth pursuing. Though our study did not yield the intended outcome, we remain firm believers in the potential of this research area.

References

Bao, X., Gjorgieva, E., Shanahan, L. K., Howard, J. D., Kahnt, T., & Gottfried, J. A. (2019). Grid-like neural representations support olfactory navigation of a two-dimensional odor space. Neuron, 102(5), 1066-1075.e5. https://doi.org/10.1016/j.neuron.2019.03.034

Barry, C., Hayman, R., Burgess, N., & Jeffery, K. J. (2007). Experience-dependent rescaling of entorhinal grids. Nature Neuroscience, 10(6), 682-684. https://doi.org/10.1038/nn1905

Baram, A. B., Muller, T. H., Nili, H., Garvert, M. M., & Behrens, T. E. J. (2020). Entorhinal and ventromedial prefrontal cortices abstract and generalize the structure of reinforcement learning problems. Neuron, 109, 1164-1178.e8. https://doi.org/10.1016/j.neuron.2020.01.038

Behrens, T. E. J., Muller, T. H., Whittington, J. C. R., Mark, S., Baram, A. B., Stachenfeld, K. L., & Kurth-Nelson, Z. (2018). What is a cognitive map? Organizing knowledge for flexible behavior. Neuron, 100(2), 490-509. doi: 10.1016/j.neuron.2018.10.002. PMID: 30359611.

Bellman, R. (1957). Dynamic Programming. Princeton University Press.

Bellmund, J. L. S., Deuker, L., Navarro Schröder, T., & Doeller, C. F. (2016). Grid-cell representations in mental simulation. eLife, 5, e17089. https://doi.org/10.7554/eLife.17089

Bellmund, J. L. S., Gärdenfors, P., Moser, E. I., & Doeller, C. F. (2018). Navigating cognition: Spatial codes for human thinking. Science, 362(6415), eaat6766. https://doi.org/10.1126/science.aat6766

Bongioanni, A., Folloni, D., Verhagen, L., Sallet, J., Klein-Flügge, M. C., & Rushworth, M. F. S. (2021). Activation and disruption of a neural mechanism for novel choice in monkeys. Nature, 591(7849), 270-274. https://doi.org/10.1038/s41586-020-03115-5

Cavanna, A. E., & Trimble, M. R. (2006). The precuneus: A review of its functional anatomy and behavioural correlates. Brain, 129(Pt 3), 564-583. https://doi.org/10.1093/brain/awl004

Chau, B. K., Kolling, N., Hunt, L. T., Walton, M. E., & Rushworth, M. F. (2014). A neural mechanism underlying failure of optimal choice with multiple alternatives. Nature Neuroscience, 17, 463-470. https://doi.org/10.1038/nn.3649

Chen, Z. S., Zhang, X., Long, X., & Zhang, S-J. (2022). Are grid-like representations a component of all perception and cognition? Frontiers in Neural Circuits, 16, 924016. https://doi.org/10.3389/fncir.2022.924016.

Chrastil, E. R., Sherrill, K. R., Hasselmo, M. E., & Stern, C. E. (2015). There and back again: Hippocampus and retrosplenial cortex track homing distance during human path integration. Journal of Neuroscience, 35(46), 15442-15452. https://doi.org/10.1523/JNEUROSCI.1209-15.2015

Constantinescu, A. O., O'Reilly, J. X., & Behrens, T. E. J. (2016). Organizing conceptual knowledge in humans with a gridlike code. Science, 352(6292), 1464-1468. https://doi.org/10.1126/science.aaf0941

Daw, N. D., Niv, Y., & Dayan, P. (2005). Uncertainty-based competition between prefrontal and dorsolateral striatal systems for behavioral control. Nature Neuroscience, 8, 1704-1711.

Daw, N. D., & Niv, Y. (2008). Model-based and model-free Pavlovian reward learning: revaluation, revision, and revelation. Cognitive, Affective, & Behavioral Neuroscience, 8(3), 333-339. https://doi.org/10.3758/CABN.8.3.333

Daw, N. D., Gershman, S. J., Seymour, B., Dayan, P., & Dolan, R. J. (2011). Model-based influences on humans' choices and striatal prediction errors. Neuron, 69(6), 1204-1215. doi: 10.1016/j.neuron.2011.02.027

Denny, B. T., Kober, H., Wager, T. D., & Ochsner, K. N. (2012). A meta-analysis of functional neuroimaging studies of self and other judgments reveals a spatial gradient for mentalizing in medial prefrontal cortex. Journal of Cognitive Neuroscience, 24(8), 1742-1752. doi: 10.1162/jocn_a_00233.

Doeller, C. F., Barry, C., & Burgess, N. (2010). Evidence for grid cells in a human memory network. Nature, 463, 657-661. https://doi.org/10.1038/nature08704

Fix, E., & Hodges, J. L. Jr. (1951). Discriminatory analysis, nonparametric discrimination: Consistency properties. Technical Report, RAND Corporation.

Fyhn, M., Hafting, T., Treves, A., Moser, M. B., & Moser, E. I. (2007). Hippocampal remapping and grid realignment in entorhinal cortex. Nature, 446, 190-194. https://doi.org/10.1038/nature05601

Garnier, S., Ross, N., Rudis, B., Sciaini, M., & Scherer, C. (2021). viridis: Default color maps from ‘matplotlib'. [Software]. Retrieved from https://cran.r-project.org/web/packages/viridis/index.html

Gorgolewski, K., Burns, C. D., Madison, C., Clark, D., Halchenko, Y. O., Waskom, M. L., & Ghosh, S. S. (2011). Nipype: A flexible, lightweight and extensible neuroimaging data processing framework in Python. Frontiers in Neuroinformatics, 5, 13. https://doi.org/10.3389/fninf.2011.00013

Hafting, T., Fyhn, M., Molden, S., Moser, M. B., & Moser, E. I. (2005). Microstructure of a spatial map in the entorhinal cortex. Nature, 436, 801-806. https://doi.org/10.1038/nature03721

Harlow, H. F. (1938). The nature of learning. Journal of General Psychology, 18(2), 149-169. https://doi.org/10.1080/00221309.1938.9713357

Harlow, H. F. (1949). The formation of learning sets. Psychological Review, 56(1), 51-65. https://doi.org/10.1037/h0062474

Hau, B., Kolling, N., Hunt, L., Rushworth, M. F. S. (2014). A neural mechanism underlying failure of optimal choice with multiple alternatives. Nature Neuroscience, 17(4), 463–470. https://doi.org/10.1038/nn.3649

Henssen, A., Zilles, K., Palomero-Gallagher, N., Schleicher, A., Mohlberg, H., Gerboga, F., ... & Amunts, K. (2016). Cytoarchitecture and probability maps of the human medial orbitofrontal cortex. Cortex, 75, 87-112. https://doi.org/10.1016/j.cortex.2015.11.006

Horner, A. J., Bisby, J. A., Wang, A., Bogus, K., & Burgess, N. (2016). The role of spatial boundaries in shaping long-term event representations. Cognition, 154, 151-164. https://doi.org/10.1016/j.cognition.2016.05.013

Kahneman, D., & Tversky, A. (1979). Prospect Theory: An Analysis of Decision under Risk. Econometrica, 47(2), 263-291.

Kubie, J. L., & Ranck, J. B. (1983). Sensory-behavioral correlates in individual hippocampus neurons in three situations: space and context. In W. Seifert (Ed.), Neurobiology of the hippocampus (pp. 433–447). Academic Press.

Long X., Deng B., Cai J., Chen Z. S., Zhang S.-J. (2021a). A compact spatial map in V2 visual cortex. BioRxiv. preprint. 10.1101/2021.02.11.430687

Marr, D. (1982). Vision: A computational investigation into the human representation and processing of visual information. MIT Press.

Montague, P. R., Dayan, P., & Sejnowski, T. J. (1996). A framework for mesencephalic dopamine systems based on predictive Hebbian learning. Journal of Neuroscience, 16(5), 1936-1947. https://doi.org/10.1523/JNEUROSCI.16-05-01936.1996

Moser, E. I., Kropff, E., & Moser, M. B. (2008). Place cells, grid cells, and the brain's spatial representation system. Annual Review of Neuroscience, 31, 69-89. https://doi.org/10.1146/annurev.neuro.31.061307.090723

Müller, N. G., Riemer, M., Brandt, L., & Wolbers, T. (2018). Repetitive transcranial magnetic stimulation reveals a causal role of the human precuneus in spatial updating. Scientific Reports, 8(1), 10171. https://doi.org/10.1038/s41598-018-28487-7

O'Doherty, J. P., Dayan, P., Friston, K., Critchley, H., & Dolan, R. J. (2003). Temporal difference models and reward-related learning in the human brain. Neuron, 38(2), 329-337.

O'Keefe, J., & Dostrovsky, J. (1971). The hippocampus as a spatial map. Preliminary evidence from unit activity in the freely-moving rat. Brain Research, 34(1), 171-175. doi: 10.1016/0006-8993(71)90358-1.

Padoa-Schioppa, C., & Assad, J. A. (2008). The representation of economic value in the orbitofrontal cortex is invariant for changes of menu. Nature Neuroscience, 11(1), 95-102. https://doi.org/10.1038/nn2020

Padoa-Schioppa, C., & Assad, J. A. (2006). Neurons in the orbitofrontal cortex encode economic value. Nature, 441(7090), 223-226. https://doi.org/10.1038/nature04676

Raichle, M. E., MacLeod, A. M., Snyder, A. Z., Powers, W. J., Gusnard, D. A., & Shulman, G. L. (2001). A default mode of brain function. Proceedings of the National Academy of Sciences, 98(2), 676-682. https://doi.org/10.1073/pnas.98.2.676.

Raithel, C., & Gottfried, J. A. (2021). What Are Grid-Like Responses Doing in the Orbitofrontal Cortex? Behavioral Neuroscience, 135(3), 218-225. https://doi.org/10.1037/bne0000453

Ranganath, C., & Ritchey, M. (2012). Two cortical systems for memory-guided behaviour. Nature Reviews Neuroscience, 13, 713-726.

Rescorla, R. A., & Wagner, A. R. (1972). A theory of Pavlovian conditioning: Variations in the effectiveness of reinforcement and nonreinforcement. In A. H. Black & W. F. Prokasy (Eds.), Classical conditioning II: Current research and theory (pp. 64-99). Appleton-Century-Crofts.

Rudebeck, P. H., Saunders, R. C., Prescott, A. T., Chau, L. S., & Murray, E. A. (2013). Prefrontal mechanisms of behavioral flexibility, emotion regulation and value updating. Nature Neuroscience, 16(8), 1140-1145. https://doi.org/10.1038/nn.3440

Schott, B. H., Wüstenberg, T., Lücke, E., Pohl, I.-M., Richter, A., Seidenbecher, C. I., Pollmann, S., Kizilirmak, J. M., & Richardson-Klavehn, A. (2019). Gradual acquisition of visuospatial associative memory representations via the dorsal precuneus. Human Brain Mapping, 40(5), 1554-1570. https://doi.org/10.1002/hbm.24467

Schuck, N. W., & Niv, Y. (2019). Sequential replay of non-spatial task states in the human hippocampus. Science, 364(6447). 1454-1458.

Schultz, W., Dayan, P., & Montague, P. R. (1997). A neural substrate of prediction and reward. Science, 275(5306), 1593-1599. https://doi.org/10.1126/science.275.5306.1593

Skinner, B. F. (1974). About behaviorism. New York, NY: Vintage Books.

Solstad, T., Boccara, C. N., Kropff, E., Moser, M.-B., & Moser, E. I. (2008). Representation of geometric borders in the entorhinal cortex. Science, 322(5909), 1865-1868.

Smith, S. M., Jenkinson, M., Woolrich, M. W., Beckmann, C. F., Behrens, T. E. J., Johansen-Berg, H., Bannister, P. R., De Luca, M., Drobnjak, I., Flitney, D. E., Niazy, R. K., Saunders, J., Vickers, J., Zhang, Y., De Stefano, N., Brady, J. M., & Matthews, P. M. (2004). Advances in functional and structural MR image analysis and implementation as FSL. NeuroImage, 23(Supplement 1), S208-S219. doi: 10.1016/j.neuroimage.2004.07.051

Stachenfeld, K. L., Botvinick, M. M., & Gershman, S. J. (2017). The hippocampus as a predictive map. Nature Neuroscience, 20, 1643-1653. doi: 10.1038/nn.4658.

Stangl, M., Shine, J., & Wolbers, T. (2017). The GridCAT: A Toolbox for Automated Analysis of Human Grid Cell Codes in fMRI. Frontiers in Neuroinformatics, 11.

Stensola, H., Stensola, T., Solstad, T., Frøland, K., Moser, M. B., & Moser, E. I. (2012). The entorhinal grid map is discretized. Nature, 492(7427), 72-78. doi: 10.1038/nature11649.

Sutton, R. S., & Barto, A. G. (1998). Reinforcement learning: An introduction. MIT Press.

Taube, J. S., Muller, R. U., & Ranck Jr, J. B. (1990). Head-direction cells recorded from the postsubiculum in freely moving rats. I. Description and quantitative analysis. Journal of Neuroscience, 10(2), 420-435.

Thorndike, E. L. (1898). Animal intelligence: An experimental study of the associative processes in animals. The Psychological Review: Monograph Supplements, 2(4), i-109.

Tolman, E. C. (1948). Cognitive maps in rats and men. Psychological Review, 55(4), 189-208.

Tolman, E. C., & Honzik, C. H. (1930). Introduction and removal of reward, and maze performance in rats. University of California Publications in Psychology, 4(5), 257-275.

Long, X., & Zhang, S.-J. (2021). A novel somatosensory spatial navigation system outside the hippocampal formation. Cell Research, 31(6), 649-663. https://doi.org/10.1038/s41422-020-00448-8

Wagner, I. C., Graichen, L. P., Todorova, B., Lüttig, A., Omer, D. B., Stangl, M., & Lamm, C. (2023). Entorhinal grid-like codes and time-locked network dynamics track others navigating through space. Nature Communications, 14, 231. https://doi.org/10.1038/s41467-022-29505-1

Whittington, J. C. R., Muller, T. H., Mark, S., Barry, C., Behrens, T. E. J., & Burgess, N. (2020). The Tolman-Eichenbaum machine: Unifying space and relational memory through generalization in the hippocampal formation. Cell, 183(5), 1249-1263.e23. https://doi.org/10.1016/j.cell.2020.10.014

Wilson, M. A., & McNaughton, B. L. (1994). Reactivation of hippocampal ensemble memories during sleep. Science, 265(5172), 676-679. doi: 10.1126/science.8036517

Yu, L. Q., Park, S. A., Sweigart, S. C., Boorman, E. D., & Nassar, M. R. (2021). Do grid codes afford generalization and flexible decision-making? bioRxiv. https://doi.org/10.1101/2021.06.14.448192

Zhang, S., Schonfeld, F., Wiskott, L., & Manahan-Vaughan, D. (2014). Spatial representations of place cells in darkness are supported by path integration and border information. Frontiers in Behavioral Neuroscience, 8, 222. https://doi.org/10.3389/fnbeh.2014.00222

Appendix

Table 3

Self-Related Trials, Decision phase > Baseline, 35 Significant Clusters

Brain region	MNI coordinates			z-value	Cluster mean	Cluster size
	x	y	z			
mOFC	-34	12	-20	-3.992	-3.56	88
L ACC	0	28	-6	-4.15788	-3.533	1392
R inf PC	40	-52	46	4.67399	3.604	3152
R inf OC	2	-84	0	4.07466	3.572	2496

Note. This table reports t clusters and corresponding MNI coordinates of peak activation voxels, aside from cluster mean and size. Effects were considered significant using cluster-based inference, with a cluster-defining threshold of $p > .001$ and a cluster size of bigger than 10 voxels, FPR correction was used to adjust for multiple comparisons.

Figure 12

Liberal Anaylsis of Self-Related Trials, Decision phase > Baseline

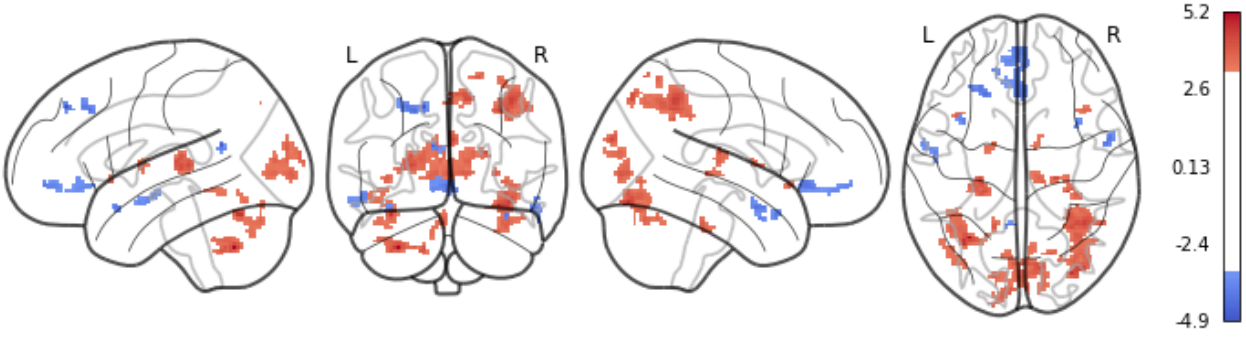

Note. Results were shown at $p < 0.001$, FPR corrected, and a minimum cluster size of 10 voxels.

Table 4

Self-Related Trials, Familiar > Novel, 2 Significant Clusters

Brain region	MNI coordinates			z-value	Cluster mean	Cluster size
	x	y	z			
Precuneus	24	-6	28	-4.416	-3.68014	136
R medial temporal gyrus	48	-36	-2	-4.352	-3.66986	112

Note. This table reports t clusters and corresponding MNI coordinates of peak activation voxels, aside from cluster mean and size. Effects were considered significant using cluster-based inference, with a cluster-defining threshold of p > .001 and a cluster size of bigger than 10 voxels, FPR correction was used to adjust for multiple comparisons.

Figure 13

Liberal Analysis of Self-Related Trials, Familiar > Novel

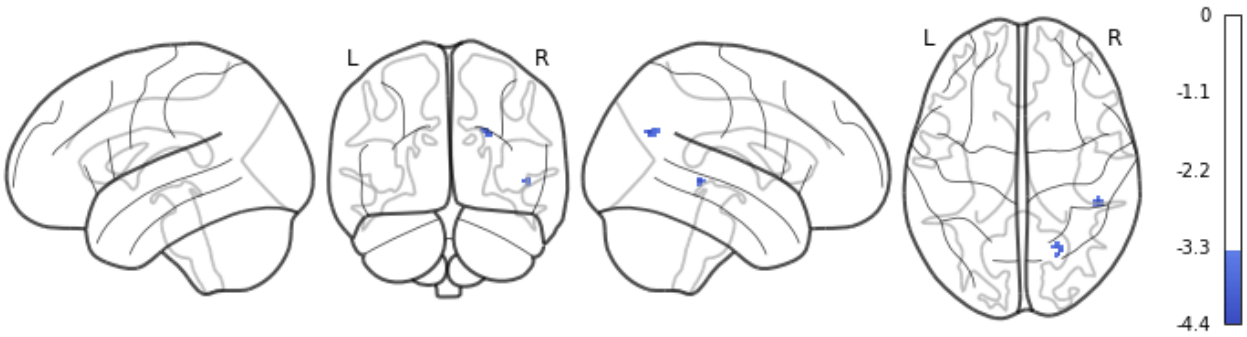

Note.The results were reported at p < 0.001, FPR corrected, and a minimum cluster size of 10 voxels. Two clusters were identified: the precuneus (x = 24, y = -68, z = 28, cluster mean = -3.680, peak = -4.416) and the right middle temporal gyrus (x = 48, y = -36, z = -2, cluster mean = -3.669, peak = -4.352).

Figure 14

Pilot Data, Accuracy and Confidence Across Sessions and Tasks

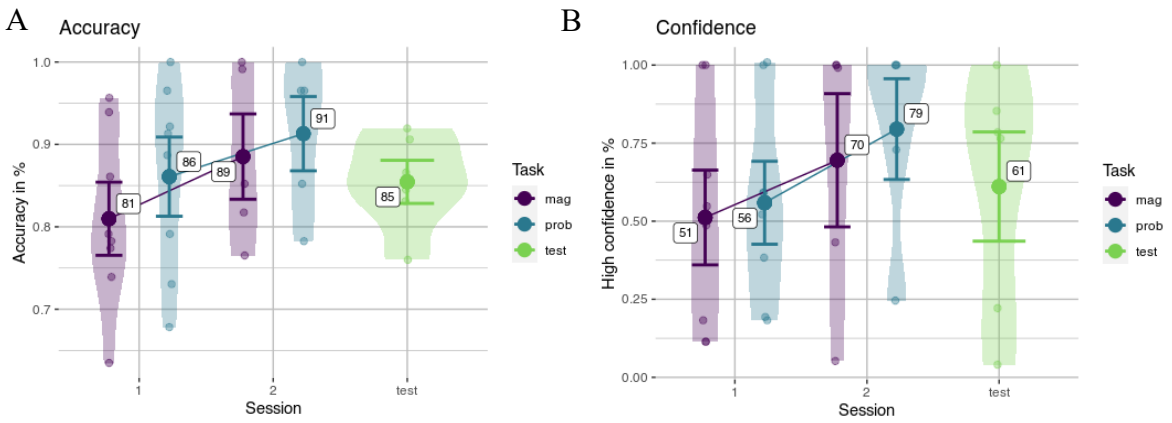

Note. Error bars represent 95% confidence intervals
Specific note. (A) steep learning curves between the training demonstrated effective progressing value asscoiations to stimuli. Similarly, high accuracy during the third session indicates active inference on novel trials.
Specific note. (B) high growth of confidence during ongoing training and decrease during introduction of novel trials reflects plausibility of our task.

Table 5

Descriptive Statistics and Correlation Coefficients of Key Behavioral Variables

Variable	M	SD	1	2	3
1. Accuracy	0.79	0.08			
2. High Confidence Proportion	0.40	0.24	.63 [-.24, .94]		
3. Reaction Time	1.99	0.58	-.69 [-.95, .13]	-.35 [-.87, .55]	
4. Inconclusiveness	2.52	0.25	.56 [-.34, .92]	.95** [.69, .99]	-38 [-.88, .53]

Note. Mean and standard deviations of behavioral measures as well as their correlation matrix. 95% confidence intervals are enclosed within square brackets.

Table 6

Wilcoxon-Mann-Whitney U Test, Familiarity Conditions

Measure	U	p	95% CI
Accuracy	19	0.535	[-0.135] [0.073]
Confidence	19	0.535	[-0.40] [0.28]
Reaction Time	20	0.662	[-1.03] [0.97]
Inconclusiveness	15	0.259	[-0.50] [0.23]

Note. As there were no significant effects observed, no adjustments for multiple comparisons were made.

Figure 16

Event File Displaying Trials Organized by Experimental Conditions.

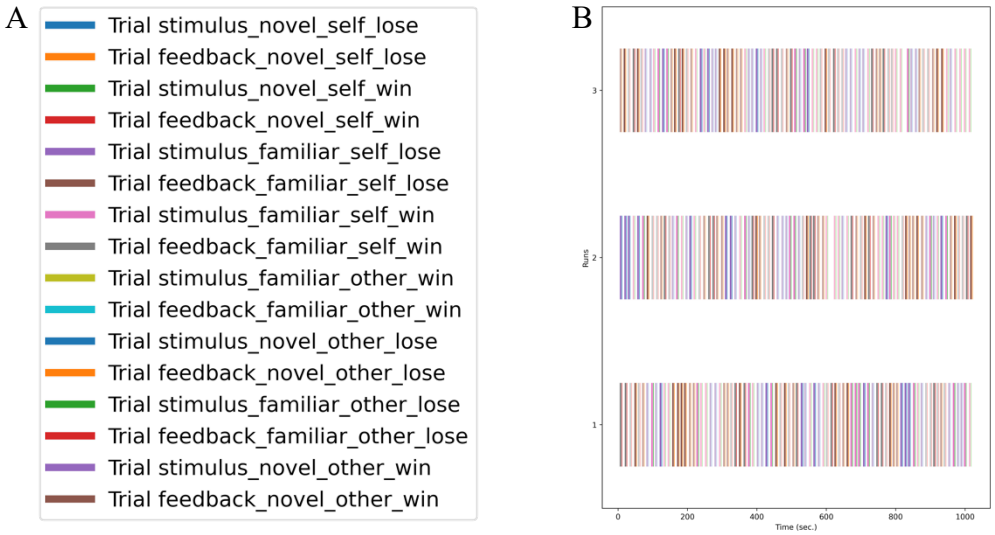

Note. (A) In the fMRI event file, trials were differentiated based on several key factors: the phase of the trial (decision or feedback), the decision context (self-related or other-related), the decision familiarity (familiar or novel), and the outcome of the decision (win or loss). (B) Eventfile of a single subject across all three runs of the decision-making task.

Figure 17

Feedback Phase, Main Effect, All Trials, Feedback > Baseline

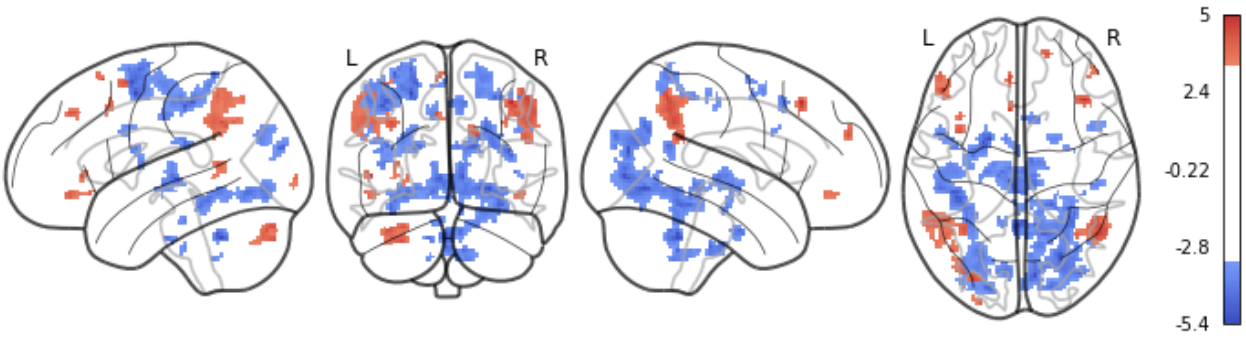

Note: The results were reported with a statistical significance threshold of $p < 0.001$, FPR corrected, and a minimum cluster size of 10 voxels. The contrast revealed significant activations in areas also associated with the decision phase, including the mOFC (x = 48, y = 44, z = -10, cluster mean = 3.869, peak = 4.016) and bilateral medial frontal gyrus (left: x = -6, y = 40, z = 40, cluster mean = 3.620, peak = 4.965; right: x = 40, y = 26, z = 46, cluster mean = 3.772, peak = 4.965)

Figure 18

Feedback Phase, All Trials, Win > Lose

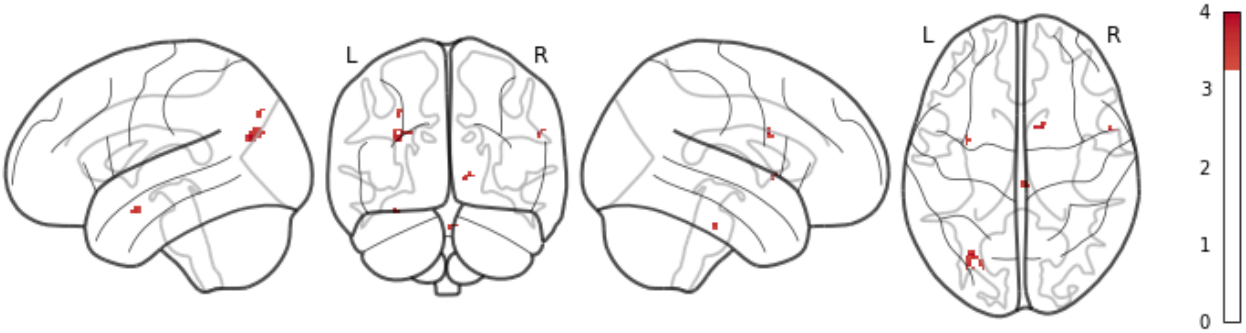

Note. Whole-brain activity during feedback conditions (win – lose) was analyzed with a low threshold to explore image plausibility. Results were shown at $p < 0.001$, FPR corrected, and a minimum cluster size of 10 voxels. The contrast analysis revealed, aside from the parietal/occipital response,significant activation in Brainstem (x = 4, y = -28, z = -30, cluster mean = 3.46, peak = 3.62), Amygdala (x = -32, y = 0, z = -22, cluster mean = 3.47, peak = 3.64), and Caudate nucleus (x = 14, y = 8, z = 0, cluster mean = 3.44, peak = 3.56). These findings confirm our expectations regarding reward processing and suggest that the images used in the study were plausible

Figure 19

Grid Magnitudes from Control Analysis, X-fold Symmetrical Models

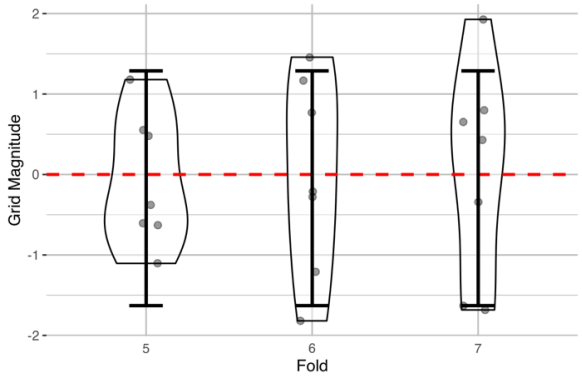

Note. The figure displayes the grid magnitudes of all rotational symmetries, these were considered for purpose of control analysis. The red-dotted line represents the zero threshold. Error bars represent 95% confidence intervals.

R-Code for Grid Estimates Analysis

```
library(data.table)
library(ggplot2)
library(ggrepel)
library(tidyr)


# Create a vector with participant IDs
participants <- paste0("GD", sprintf("%02d", 1:7))


# Function to create the file path for each participant and fold
create_filepath <- function(participant, metric, fold_dir) {
  paste0("~",
         participant, "/output/", fold_dir, "/", participant, "_GridMetric_",
metric, ".txt")
}


# Load the within-grid_orientation data for each participant into a list of d
ata.tables for 5fold, 6fold, and 7fold
within_grid_orientation_list <- lapply(participants, function(p) {
  l <- list()
  for (fd in c("5fold", "6fold", "7fold")) {
    file_path <- create_filepath(p, 3, fd)
    data <- fread(file_path, sep = ";", header = FALSE, drop = 10)
    colnames(data) <- c("GRID_METRIC", "X-FOLD_SYMMETRY", "ROI", "VOXEL-WISE_
GRID_ORI_IMAGE_1", "VOXEL-WISE_GRID_ORI_IMAGE_2", "%_STABLE_VOXELS_WITHIN_ROI
", "IMAGE_1_VOXELS_WITHIN_ROI", "IMAGE_2_VOXELS_WITHIN_ROI", "IMAGE_1_NaN_VOX
ELS_WITHIN_ROI", "IMAGE_2_NaN_VOXELS_WITHIN_ROI")
    data <- data[-1,] # Remove the first row containing the header informatio
n
    data[, PARTICIPANT := p]
    l[[fd]] <- data
  }
  return(l)
})


# Load the grid_magnitude data for each participant into a list of data.table
s for 5fold, 6fold, and 7fold
```

```
grid_magnitude_list <- lapply(participants, function(p) {
  l <- list()
  for (fd in c("5fold", "6fold", "7fold")) {
    file_path <- create_filepath(p, 1, fd)
    data <- fread(file_path, sep = ";", header = FALSE, drop = 8)
    colnames(data) <- c("GRID_METRIC", "X-FOLD_SYMMETRY", "ROI", "CONTRAST_NU
MBER",
                        "CONTRAST_NAME", "MEAN_CON-VALUE_WITHIN_ROI", "VOXELS
_WITHIN_ROI",
                        "NaN_VOXELS_WITHIN_ROI")
    data <- data[-1,] # Remove the first row containing the header informatio
n
    data[, PARTICIPANT := p]

    l[[fd]] <- data
  }
  return(l)
})


# Loading the grid_coherence data for each participant into a list of data.ta
bles for 5fold, 6fold, and 7fold
grid_coherence_list <- lapply(participants, function(p) {
  l <- list()
  for (fd in c("5fold", "6fold", "7fold")) {
    file_path <- create_filepath(p, 2, fd)
    data <- fread(file_path, sep = ";", header = FALSE, drop = 8) # Read the
data without headers
    colnames(data) <- c("GRID_METRIC", "X-FOLD_SYMMETRY", "ROI", "VOXEL-WISE_
GRID_ORI_IMAGE", "RAYLEIGH_z", "RAYLEIGH_p", "VOXELS_WITHIN_ROI", "NaN_VOXELS
_WITHIN_ROI")
    data <- data[-1,] # Remove the first row containing the header
    data[, PARTICIPANT := p]
    l[[fd]] <- data
  }
  return(l)
})
```

```
# Load the mean grid orientation data for each participant into a list of dat
a.tables for 5fold, 6fold, and 7fold
mean_grid_orientation_list <- lapply(participants, function(p) {
  l <- list()
  for (fd in c("5fold", "6fold", "7fold")) {
    file_path <- create_filepath(p, 4, fd)
    data <- fread(file_path, sep = ";", header = FALSE, drop = 7) # Read the
data without headers
    colnames(data) <- c("GRID_METRIC", "X-FOLD_SYMMETRY", "ROI", "GRID_EVENT"
, "RUN", "MEAN_GRID_ORI_IN_DEGREES_VOXELS_WEIGHTED", "MEAN_GRID_ORI_IN_DEGREE
S_VOXELS_NOT_WEIGHTED")
    data <- data[-1,] # Remove the first row containing the header informatio
n
    data[, PARTICIPANT := p]
    l[[fd]] <- data
  }
  return(l)
})


# Combine all data tables within each list for each fold
combined_within_grid_orientation <- lapply(within_grid_orientation_list, func
tion(l) {
  rbindlist(l)
})


combined_grid_magnitude <- lapply(grid_magnitude_list, function(l) {
  rbindlist(l)
})


combined_grid_coherence <- lapply(grid_coherence_list, function(l) {
  rbindlist(l)
})


combined_mean_grid_orientation <- lapply(mean_grid_orientation_list, function
(l) {
  rbindlist(l)
})
```

```
# Add a column for fold information to each combined data table
for (i in seq_along(combined_within_grid_orientation)) {
  combined_within_grid_orientation[[i]][, FOLD := c("5fold", "6fold", "7fold"
)[i]]
}

for (i in seq_along(combined_grid_magnitude)) {
  combined_grid_magnitude[[i]][, FOLD := c("5fold", "6fold", "7fold")[i]]
}

for (i in seq_along(combined_grid_coherence)) {
  combined_grid_coherence[[i]][, FOLD := c("5fold", "6fold", "7fold")[i]]
}

for (i in seq_along(combined_mean_grid_orientation)) {
  combined_mean_grid_orientation[[i]][, FOLD := c("5fold", "6fold", "7fold")[
i]]
}

# Combine all data tables into a single data frame for each metric
combined_within_grid_orientation <- rbindlist(combined_within_grid_orientatio
n)
combined_grid_magnitude <- rbindlist(combined_grid_magnitude)
combined_grid_coherence <- rbindlist(combined_grid_coherence)
combined_mean_grid_orientation <- rbindlist(combined_mean_grid_orientation)



#-----------------------------------------


# grid magnitudes


#-----------------------------------------
```

```
# Filter the data for allRuns_decision_self_novel-PMOD-alignmentWithROI1meanOri
mag_vals <- combined_grid_magnitude[CONTRAST_NAME == "allRuns_decision_self_novel-PMOD-alignmentWithROI1meanOri", .(PARTICIPANT, FOLD = `X-FOLD_SYMMETRY`, MEAN_CON_VALUE = `MEAN_CON-VALUE_WITHIN_ROI`)]



# Calculate the confidence intervals and mean values for each fold
conf_int_list <- by(mag_vals$MEAN_CON_VALUE, mag_vals$FOLD, function(x) {
  wilcox.test(x, mu = 0, conf.int = TRUE, conf.level = 0.95)$conf.int
})
mean_values <- by(mag_vals$MEAN_CON_VALUE, mag_vals$FOLD, mean)


# Add the calculated values to the mag_vals data.frame
mag_vals$conf_int <- unlist(conf_int_list)[as.numeric(mag_vals$FOLD)]
mag_vals$mean_value <- unlist(mean_values)[as.numeric(mag_vals$FOLD)]


# Create the plot
plot <- ggplot(mag_vals, aes(x = factor(FOLD), y = MEAN_CON_VALUE)) +
  geom_violin(aes(y = MEAN_CON_VALUE), show.legend = FALSE, color = "black", alpha = 0.5, width = 0.5) +
  geom_point(aes(x = factor(FOLD), y = MEAN_CON_VALUE), alpha = 0.4, size = 2, position = position_jitter(width = 0.1), color = "black") +
  labs(x = "Fold",
       y = "Grid Magnitude") +
  theme(legend.position = "none",
        panel.background = element_blank(),
        panel.grid = element_line(color = "gray"),
        panel.grid.minor.x = element_blank(),
        axis.ticks.x = element_blank(),
        axis.text.x = element_text(),
        plot.title = element_text(hjust = 0.5, size = 14, face = "bold")) +
  geom_hline(yintercept = 0, color = "red", linetype = "dashed", size = 1) +
  geom_errorbar(aes(x = factor(FOLD), ymin = conf_int[1], ymax = conf_int[2]), width = 0.2, size = 1, alpha = 0.6, color = "black") +
  geom_point(aes(x = factor(FOLD), y = mean_value), color = "black", size = 4, alpha = 0.4)
```

```
# Display the plot
plot



# Calculate the Wilcoxon signed-rank test for the 6th fold
fold6_test <- wilcox.test(mag_vals[mag_vals$FOLD == 6, ]$MEAN_CON_VALUE, mu =
0)


# Create the plot
plot <- ggplot(mag_vals, aes(x = factor(FOLD), y = MEAN_CON_VALUE)) +
  geom_violin(aes(y = MEAN_CON_VALUE), show.legend = FALSE, color = "black",
alpha = 0.5, width = 0.5) +
  geom_point(aes(x = factor(FOLD), y = MEAN_CON_VALUE), alpha = 0.4, size = 2
, position = position_jitter(width = 0.1), color = "black") +
  labs(title = "Grid Magnitude",
       x = "Fold",
       y = "Grid Magnitude") +
  theme(legend.position = "none",
        panel.background = element_blank(),
        panel.grid = element_line(color = "gray"),
        panel.grid.minor.x = element_blank(),
        axis.ticks.x = element_blank(),
        axis.text.x = element_text(),
        plot.title = element_text(hjust = 0.5, size = 14, face = "bold")) +
  geom_hline(yintercept = 0, color = "red", linetype = "dashed", size = 1) +
  geom_errorbar(aes(x = factor(FOLD), ymin = conf_int[1], ymax = conf_int[2])
, width = 0.2, size = 1, alpha = 0.6, color = "black") +
  geom_point(aes(x = factor(FOLD), y = mean_value), color = "black", size = 4
, alpha = 0.4) +
  annotate("text", x = 6, y = max(mag_vals[mag_vals$FOLD == 6, ]$MEAN_CON_VAL
UE) + 0.25,
           label = paste("W =", round(fold6_test$statistic, 2), ", p =", roun
d(fold6_test$p.value, 4)),
           hjust = 2.5, vjust = 1.4, color = "black")


# Display the plot
```

```
plot



#-----------------------------------------


# between voxel coherence, spatial stability


#-----------------------------------------


# Combine coherence and magnitude data
combined_data <- merge(coherence_vals, mag_vals, by = "PARTICIPANT")


# Calculate correlation and p-value
correlation <- cor.test(combined_data$coherence, combined_data$MEAN_CON_VALUE
)


# Create plot with regression line, correlation, and p-value
plot <- ggplot(combined_data, aes(x = coherence, y = MEAN_CON_VALUE)) +
  geom_point() +
  geom_smooth(method = "lm", se = TRUE, color = "blue") +
  labs(x = "Rayleigh's z", y = "Grid Matnitude Estimate") +
  ggtitle("") +
  theme_bw() +
  theme(plot.title = element_text(hjust = 0.5)) +
  annotate("text", x = min(combined_data$coherence), y = max(combined_data$ME
AN_CON_VALUE),
           label = paste("r = ", round(correlation$estimate, 2), ", p-value =
", round(correlation$p.value, 4), sep = ""),
           hjust = -1, vjust = -3, size = 4)


# Display plot
print(plot)


#-----------------------------------------


# pairwise within voxel cohrence, temporal stability
```

```
#-----------------------------------------



within_voxel_run_1_3 <- combined_within_grid_orientation[`VOXEL-WISE_GRID_ORI
_IMAGE_1` == "voxelwiseGridOri_decision_self_novel_run1_deg.nii"
                                                         & `VOXEL-WISE_GRID_O
RI_IMAGE_2` == "voxelwiseGridOri_decision_self_novel_run3_deg.nii" , .(PARTIC
IPANT,`%_STABLE_VOXELS_WITHIN_ROI`)]



within_voxel_run_1_2 <- combined_within_grid_orientation[`VOXEL-WISE_GRID_ORI
_IMAGE_1` == "voxelwiseGridOri_decision_self_novel_run1_deg.nii"
                                                         & `VOXEL-WISE_GRID_O
RI_IMAGE_2` == "voxelwiseGridOri_decision_self_novel_run2_deg.nii" , .(PARTIC
IPANT,`%_STABLE_VOXELS_WITHIN_ROI`)]



within_voxel_run_2_3 <- combined_within_grid_orientation[`VOXEL-WISE_GRID_ORI
_IMAGE_1` == "voxelwiseGridOri_decision_self_novel_run2_deg.nii"
                                                         & `VOXEL-WISE_GRID_O
RI_IMAGE_2` == "voxelwiseGridOri_decision_self_novel_run3_deg.nii" , .(PARTIC
IPANT,`%_STABLE_VOXELS_WITHIN_ROI`)]



# Combine the three subsets of data

combined_within_voxel <- rbind(within_voxel_run_1_3, within_voxel_run_1_2, wi
thin_voxel_run_2_3)

combined_within_voxel <- combined_within_voxel[,mean(`%_STABLE_VOXELS_WITHIN_
ROI`), by = PARTICIPANT]


# Calculate the mean of %_STABLE_VOXELS_WITHIN_ROI

mean_within_voxel <- mean(combined_within_voxel$V1)

sd_within_voxel <- sd(combined_within_voxel$V1)


# mean and sd for within_voxel_run_1_3

mean_within_voxel_run_1_3 <- mean(within_voxel_run_1_3$`%_STABLE_VOXELS_WITHI
N_ROI`)
```

```
sd_within_voxel_run_1_3 <- sd(within_voxel_run_1_3$`%_STABLE_VOXELS_WITHIN_ROI`)


# mean and sd for within_voxel_run_1_Allruns

mean_within_voxel_run_1_2 <- mean(within_voxel_run_1_2$`%_STABLE_VOXELS_WITHIN_ROI`)

sd_within_voxel_run_1_2 <- sd(within_voxel_run_1_2$`%_STABLE_VOXELS_WITHIN_ROI`)



mean_within_voxel_run_2_3 <- mean(within_voxel_run_2_3$`%_STABLE_VOXELS_WITHIN_ROI`)

sd_within_voxel_run_2_3 <- sd(within_voxel_run_2_3$`%_STABLE_VOXELS_WITHIN_ROI`)


#-----------------------------------------

# cobined within voxel cohrence, temporal stability

#-----------------------------------------


#merge

combined_data <- merge(combined_within_voxel, mag_vals, by = "PARTICIPANT")

combined_data <- combined_data[, !"x"]



# Calculate correlation and p-value

correlation <- cor.test(combined_data$V1, combined_data$MEAN_CON_VALUE)


# Create plot with regression line, correlation, and p-value

plot <- ggplot(combined_data, aes(x = V1, y = MEAN_CON_VALUE)) +

  geom_point() +

  geom_smooth(method = "lm", se = TRUE, color = "blue") +

  labs(x = "% Stable Voxels Within ROI", y = "Grid Magnitude Estimate") +

  ggtitle("") +

  theme_bw() +

  theme(plot.title = element_text(hjust = 0.5)) +

  annotate("text", x = min(combined_data$V1), y = max(combined_data$MEAN_CON_VALUE),
```

```
            label = paste("r = ", round(correlation$estimate, 2), ", p-value =
", round(correlation$p.value, 4), sep = ""),
            hjust = -1, vjust = -2, size = 4)
# Display plot
print(plot)
```

R-Code for Balancing

```
balancing_function <-
  function(nTrial = 24,fam_prop = 0.5,max_pair_repeat = 1,
           max_stim_repeat_fam = 4,max_stim_repeat_nov = 4,alpha = 0.05,
           angular_resolution = 100,num_bins = 6, bin_width = 10) {


    #libraries
    library(data.table)
    library(NISTunits)


    #parameters
    max_stim_repeat_side_nov = max_stim_repeat_nov / 2
    max_stim_repeat_side_fam = max_stim_repeat_fam / 2
    nov_prop = 1 - fam_prop

    #functions ------------------------------------------------------------
--


   #important for 2D indexing
     multi.which <- function(A) {
      if (is.vector(A))
        return(which(A))
      d <- dim(A)
      T <- which(A) - 1
      nd <- length(d)
      t(sapply(T, function(t) {
```

```
    I <- integer(nd)
    I[1] <- t %% d[1]
    sapply(2:nd, function(j) {
      I[j] <<- (t %/% prod(d[1:(j - 1)])) %% d[j]
    })
    I
  }) + 1)
}

# assesing the dimnesionality condition of trials
dim_condition <- function(indA, indB) {
  mag_1 = mag_matrix[indA]
  mag_2 = mag_matrix[indB]
  prob_1 = prob_matrix[indA]
  prob_2 = prob_matrix[indB]

  if (mag_1 > mag_2 &
      prob_1 > prob_2 | mag_2 > mag_1 & prob_2 > prob_1) {
    dim = "consistent"
  } else if (mag_1 != mag_2 &
             prob_1 == prob_2 |
             mag_1 == mag_2 & prob_1 != prob_2) {
    dim = "1-dimensional"

  } else if (mag_1 > mag_2 &
             prob_1 < prob_2 | mag_2 > mag_1 & prob_2 < prob_1 |
             mag_1 < mag_2 &
             prob_1 > prob_2 |
             mag_2 < mag_1 & prob_2 > prob_1) {
    dim = "inconsistent"
  }
  return (dim)
}
```

```
    # Function to create a list of equal counters
    create_counter_list <- function(names, value) {
      counter_list <- list()
      for (name in names) {
        counter_list[[name]] <- value
      }
      return(counter_list)
    }



    # Function to create bins
    create_bins <- function(start_angle, num_bins, bin_width, angular_resolut
ion) {
      b <- seq(0, angular_resolution - 0.01, length.out = angular_resolution)
      bins <- list()

      for (i in 1:num_bins) {
        bin_angles <- b + start_angle
        bins[[i]] <- c(bin_angles, bin_angles * -1)
        start_angle <- start_angle + bin_width
      }

      return(bins)
    }

    elementwise.all.equal <-
      Vectorize(function(x, y) {
        isTRUE(all.equal(x, y, tolerance = 0.01))
      })

    create_matrix <- function(nrow, ncol, value = 0) {
      matrix(value, nrow, ncol)
    }

    # Function to update counters
```

```
    update_counters <- function(counters, key, value = -1) {
      counters[[key]] <- counters[[key]] + value
      return(counters)
    }

    # Function to update matrices
    update_matrices <- function(matrices, n, ind_self, ind_other, stim_matrix
,
                                value_matrix, dim_self, dim_other,
                                dx_self, dy_self, dx_other, dy_other,
                                bin_s, bin_o, angle_s, angle_o) {
      keys_self <- c("sample_self", "stim1_self", "stim1_self_ind",
                     "stim2_self", "stim2_self_ind", "value1_self",
                     "value2_self", "mag_1_self", "mag_2_self", "prob_1_self"
, "prob_2_self")
      keys_other <- c("sample_other", "stim1_other", "stim1_other_ind",
                      "stim2_other", "stim2_other_ind", "value1_other",
                      "value2_other", "mag_1_other", "mag_2_other",
                      "prob_1_other", "prob_2_other")
      keys_common <- c("trial", "dim_condition_self", "dim_condition_other",
                       "distance_self", "distance_other", "bin_self", "bin_ot
her",
                       "angle_self", "angle_other")

      for (key in keys_self) {
        matrices[[key]][, n] <- ind_self
      }
      for (key in keys_other) {
        matrices[[key]][, n] <- ind_other
      }
      for (key in keys_common) {
        matrices[[key]][n] <- ifelse(grepl("self", key), ind_self, ind_other)
      }

      matrices$distance_self[n] <- sqrt(dx_self^2 + dy_self^2)
      matrices$distance_other[n] <- sqrt(dx_other^2 + dy_other^2)
```

```
      matrices$bin_self[n] <- bin_s
      matrices$bin_other[n] <- bin_o

      matrices$angle_self[n] <- angle_s
      matrices$angle_other[n] <- angle_o

      return(matrices)
    }


  # prepraration-----------------------------------------------------------
--
    -
    # Create bins
    bins <- create_bins(0, num_bins, bin_width, angular_resolution)

    # Access bins using the index
    bin1 <- bins[[1]]
    bin2 <- bins[[2]]
    bin3 <- bins[[3]]
    bin4 <- bins[[4]]
    bin5 <- bins[[5]]
    bin6 <- bins[[6]]

    #start main loop
    while (TRUE) {

      # Calculate the number of trials for each condition
      fam_nTrial <- as.integer(nTrial * fam_prop)
      nov_nTrial <- as.integer(nTrial * nov_prop)
      dim_fam_nTrial <- as.integer(fam_nTrial / 3)
      dim_nov_nTrial <- as.integer(nov_nTrial / 3)
      bin_nTrial <- as.integer(nTrial / 6)
```

```
      # Define counter names
      dim_counter_names <- c("consistent", "1-dimensional", "inconsistent")
      bin_counter_names <- paste0("bin", 1:6)

      # Initialize counters
      fam_counter_self <- list("familiar" = fam_nTrial, "novel" = nov_nTrial)
      fam_counter_other <- fam_counter_self

      dim_counter_novel_self <- create_counter_list(dim_counter_names, dim_no
v_nTrial)
      dim_counter_novel_other <- dim_counter_novel_self
      dim_counter_fam_self <- create_counter_list(dim_counter_names, dim_fam_
nTrial)
      dim_counter_fam_other <- dim_counter_fam_self

      bin_counter_self <- create_counter_list(bin_counter_names, bin_nTrial)
      bin_counter_other <- bin_counter_self



      # Initialize stimuli space
      stim_matrix <- t(matrix(rep(1:100), nrow = 10, ncol = 10))
      mag_matrix <- t(matrix(rep(c(1:10), each = 10), 10, 10))
      prob_matrix <- t(matrix(rep(seq(0.1:1, by = 0.1), 10), 10, 10))
      value_matrix <- mag_matrix * prob_matrix
      familiar_stim <- c(stim_matrix[5,], stim_matrix[, 6])

      nTrial <- 100  # Replace with your desired number of trials

      # Define matrix names
      mat_names <- c("stim1_self_ind", "stim2_self_ind",
                     "stim1_other_ind", "stim2_other_ind",
                     "sample_self", "sample_other","trial",
                     "stim1_self", "stim2_self", "stim1_other", "stim2_other"
,
                     "value1_self", "value2_self", "value1_other", "value2_ot
her",
```

```
                      "mag_1_self", "mag_2_self", "prob_1_self", "prob_2_self"
,
                      "mag_1_other", "mag_2_other", "prob_1_other","prob_2_oth
er"
                      "fam_condition_self", "fam_condition_other",
                      "dim_condition_self", "dim_condition_other",
                      "distance_self", "distance_other",
                      "bin_self", "bin_other",
                      "angle_self", "angle_other")

      # Initialize matrices
      matrices <- list()
      for (name in mat_names) {
        matrices[[name]] <- if (name == "trial") create_matrix(nTrial) else c
reate_matrix(2,

nTrial)
      }



      # exclude stimuli outside of training value range
      mag_training_values = value_matrix[5,]
      prob_training_values = value_matrix[, 6]
      range = range(c(mag_training_values, prob_training_values))

      excludedByRange_ind = which(value_matrix < range[1] |
                                    value_matrix > range[2])
      excludedByRange = t(stim_matrix[excludedByRange_ind])



      #sampling familiar trials
      for (n in 1:fam_nTrial) {
        while (TRUE) {
          sample_s = sample(familiar_stim, size = 2, replace = FALSE)
          sample_o = sample(familiar_stim, size = 2, replace = FALSE)
```

```
          if (sample_s[1] == sample_s[2] |
              sample_o[1] == sample_o[2]) {
            next
          }

          if ((sum(sample_s == sample_self) / 2) > max_pair_repeat |
              (sum(sample_o == sample_other) / 2) > max_pair_repeat) {
            next
          }

          if (length(which(stim1_self == sample_s[1])) > max_stim_repeat_side
_fam |
              length(which(stim2_self == sample_s[2])) > max_stim_repeat_side
_fam) {
            next
          } else if (length(which(stim1_other == sample_o[1])) > max_stim_rep
eat_side_fam |
                     length(which(stim2_other == sample_o[2])) > max_stim_rep
eat_side_fam) {
            next
          }

          #angles -> x-axis/columns = probability,y-axis/rows = magnitude
          ind_1_self <-
            multi.which(stim_matrix == sample_s[1])
          ind_2_self <- multi.which(stim_matrix == sample_s[2])
          ind_1_other <- multi.which(stim_matrix == sample_o[1])
          ind_2_other <- multi.which(stim_matrix == sample_o[2])

          dy_self = ind_1_self[1] - ind_2_self[1]
          dx_self = ind_1_self[2] - ind_2_self[2]
          dy_other = ind_1_other[1] - ind_2_other[1]
          dx_other = ind_1_other[2] - ind_2_other[2]

          dim_self = dim_condition(ind_1_self, ind_2_self)
          dim_other = dim_condition(ind_1_other, ind_2_other)
```

```
dy_self = sqrt((dy_self) ** 2) # half circle
dy_other = sqrt((dy_other) ** 2)

angle_s = NISTradianTOdeg(atan(dy_self / dx_self)) #
angle_o = NISTradianTOdeg(atan(dy_other / dx_other))

if (dx_self < 0) {
  angle_s = 180 + angle_s
}

if (dx_other < 0) {
  angle_o = 180 + angle_o
}

angle_s = round(angle_s, digits = 2)
angle_o = round(angle_o, digits = 2)

if (any(elementwise.all.equal(angle_s, bin1))) {
  bin_s = "bin1"
} else if (any(elementwise.all.equal(angle_s, bin2))) {
  bin_s = "bin2"
} else if (any(elementwise.all.equal(angle_s, bin3))) {
  bin_s = "bin3"
} else if (any(elementwise.all.equal(angle_s, bin4))) {
  bin_s = "bin4"
} else if (any(elementwise.all.equal(angle_s, bin5))) {
  bin_s = "bin5"
} else if (any(elementwise.all.equal(angle_s, bin6))) {
  bin_s = "bin6"
} else{
  print("fam, wrong")
  print(angle_s)
  next
```

```
          }

          if (any(elementwise.all.equal(angle_o, bin1))) {
            bin_o = "bin1"
          } else if (any(elementwise.all.equal(angle_o, bin2))) {
            bin_o = "bin2"
          } else if (any(elementwise.all.equal(angle_o, bin3))) {
            bin_o = "bin3"
          } else if (any(elementwise.all.equal(angle_o, bin4))) {
            bin_o = "bin4"
          } else if (any(elementwise.all.equal(angle_o, bin5))) {
            bin_o = "bin5"
          } else if (any(elementwise.all.equal(angle_o, bin6))) {
            bin_o = "bin6"
          } else{
            print("no bin other")
            print(angle_o)
            next
          }

          #familiar bins
          if (bin_counter_other[[1]] == 0 &
              bin_counter_other[[3]] == 0 &
              bin_counter_other[[6]] == 0 &
              dim_counter_fam_other[["1-dimensional"]] != 0) {
            break
          }

          #
          if (dim_counter_fam_self[[dim_self]] > 0 & dim_counter_fam_other[[d
im_other]] > 0) {
            if (bin_counter_self[[bin_s]] > 0 & bin_counter_other[[bin_o]] >
0) {
              if (angle_s == angle_o) {
```

```
                #save trial data and update counters
                fam_condition_self[n] <- "familiar"
                fam_condition_other[n] <- "familiar"

                bin_counter_self <- update_counters(bin_counter_self, bin_s)
                bin_counter_other <- update_counters(bin_counter_other, bin_o
)

                dim_counter_fam_self <- update_counters(dim_counter_fam_self,
dim_self)
                dim_counter_fam_other <- update_counters(dim_counter_fam_othe
r, dim_other)

                fam_counter_self <- update_counters(fam_counter_self, fam_con
dition_self[n])
                fam_counter_other <- update_counters(fam_counter_other,
                                                     fam_condition_other[n])

                matrices <- update_matrices(matrices, n, ind_self, ind_other,
stim_matrix,
                                            value_matrix, dim_self, dim_other
, dx_self,
                                            dy_self, dx_other, dy_other, bin_
s, bin_o,
                                            angle_s, angle_o)

                break
              } else {
                next
              }
            }
          }


      # novel
      for (n in (fam_nTrial + 1):nTrial) {
        while (TRUE) {
```

```
          sample_s = sample(stim_matrix, size = 2, replace = FALSE)
          sample_o = sample(stim_matrix, size = 2, replace = FALSE)

          if (any(
            sample_s %in% stim1_other | sample_s %in% stim2_other |
            sample_s %in% excludedByRange
          )) {
            next
          } else if (any(
            sample_o %in% stim1_self | sample_o %in%  stim2_self |
            sample_o %in% excludedByRange
          )) {
            next
          } else if (any(sample_s %in% familiar_stim |
                         sample_o %in% familiar_stim)) {
            next
          } else if ((sum(sample_s == sample_self) / 2) > max_pair_repeat |
                     (sum(sample_o == sample_other) / 2) > max_pair_repeat) {
            next
          } else if (length(which(stim1_self == sample_s[1])) > max_stim_repe
at_side_nov |
                     length(which(stim2_self == sample_s[2])) > max_stim_repe
at_side_nov) {
            next
          } else if (length(which(stim1_other == sample_o[1])) > max_stim_rep
eat_side_nov |
                     length(which(stim2_other == sample_o[2])) > max_stim_rep
eat_side_nov) {
            next
          }

          ind_1_self <- multi.which(stim_matrix == sample_s[1])
          ind_2_self <- multi.which(stim_matrix == sample_s[2])
          ind_1_other <- multi.which(stim_matrix == sample_o[1])
          ind_2_other <- multi.which(stim_matrix == sample_o[2])
```

```
dy_self = ind_1_self[1] - ind_2_self[1]
dx_self = ind_1_self[2] - ind_2_self[2]
dy_other = ind_1_other[1] - ind_2_other[1]
dx_other = ind_1_other[2] - ind_2_other[2]

dim_self = dim_condition(ind_1_self, ind_2_self)
dim_other = dim_condition(ind_1_other, ind_2_other)

dy_self = sqrt((dy_self) ** 2)
dy_other = sqrt((dy_other) ** 2)

angle_s = NISTradianTOdeg(atan(dy_self / dx_self))
angle_o = NISTradianTOdeg(atan(dy_other / dx_other))

if (dx_self < 0) {
  angle_s = 180 + angle_s
}

if (dx_other < 0) {
  angle_o = 180 + angle_o
}

angle_s = round(angle_s, digits = 2)
angle_o = round(angle_o, digits = 2)

if (any(elementwise.all.equal(angle_s, bin1))) {
  bin_s = "bin1"
} else if (any(elementwise.all.equal(angle_s, bin2))) {
  bin_s = "bin2"
} else if (any(elementwise.all.equal(angle_s, bin3))) {
  bin_s = "bin3"
} else if (any(elementwise.all.equal(angle_s, bin4))) {
  bin_s = "bin4"
} else if (any(elementwise.all.equal(angle_s, bin5))) {
```

```
    bin_s = "bin5"
  } else if (any(elementwise.all.equal(angle_s, bin6))) {
    bin_s = "bin6"
  } else{
    print("novel, no bin")
    # next
  }

  if (any(elementwise.all.equal(angle_o, bin1))) {
    bin_o = "bin1"
  } else if (any(elementwise.all.equal(angle_o, bin2))) {
    bin_o = "bin2"
  } else if (any(elementwise.all.equal(angle_o, bin3))) {
    bin_o = "bin3"
  } else if (any(elementwise.all.equal(angle_o, bin4))) {
    bin_o = "bin4"
  } else if (any(elementwise.all.equal(angle_o, bin5))) {
    bin_o = "bin5"
  } else if (any(elementwise.all.equal(angle_o, bin6))) {
    bin_o = "bin6"
  } else{
    print("no bin other")
  }

  if (angle_s == angle_o) {
    #bin_s == bin_o?

    dim_self = dim_condition(ind_1_self, ind_2_self)
    dim_other = dim_condition(ind_1_other, ind_2_other)

    if (bin_counter_other[[1]] == 0 &
        bin_counter_other[[3]] == 0 &
        bin_counter_other[[6]] == 0 &
        dim_counter_novel_other[["1-dimensional"]] != 0) {
```

```
            break
          }

          if (dim_counter_novel_self[[dim_self]] > 0 &
              dim_counter_novel_other[[dim_other]] > 0 &
              fam_counter_self[["novel"]] > 0 &
              fam_counter_other[["novel"]] > 0) {
            if (bin_counter_self[[bin_s]] > 0 &
                bin_counter_other[[bin_o]] > 0) {

              # Update counters
              bin_counter_self <- update_counters(bin_counter_self, bin_s)
              bin_counter_other <- update_counters(bin_counter_other, bin_o
)
              dim_counter_novel_self <- update_counters(dim_counter_novel_s
elf, dim_self)
              dim_counter_novel_other <- update_counters(dim_counter_novel_
other,
                                                         dim_other)
              fam_counter_self <- update_counters(fam_counter_self, "novel"
)
              fam_counter_other <- update_counters(fam_counter_other, "nove
l")

              # Update matrices
              matrices <- update_matrices(matrices, n, ind_1_self, ind_1_ot
her,
                                          stim_matrix,value_matrix, dim_sel
f, dim_other,
                                          dx_self, dy_self, dx_other, dy_ot
her, bin_s,
                                          bin_o, angle_s, angle_o)

              matrices$dim_condition_self[n] <- dim_self
              matrices$dim_condition_other[n] <- dim_other
              matrices$fam_condition_self[n] <- "novel"
              matrices$fam_condition_other[n] <- "novel"
```

```
                break
              } else{
                next
              }
            } else{
              next
            }
          } else{
            next
          }
        }
      }

      # create data table
      dt <-
        data.table(
          "trial" = rep(trial, 2),
          "stim1" = c(stim1_self, stim1_other),
          "stim2" = c(stim2_self, stim2_other),
          "mag1" = c(mag_1_self, mag_1_other),
          "mag2" = c(mag_2_self, mag_2_other),
          "prob1" = c(prob_1_self, prob_1_other),
          "prob2" = c(prob_2_self, prob_2_other),
          "value1" = c(value1_self, value1_other),
          "value2" = c(value2_self, value2_other),
          "social" = c(rep("self", length(stim1_self)), rep("other", length
(stim1_other))),
          "dim" = c(dim_condition_self, dim_condition_other),
          "fam" = c(fam_condition_self, fam_condition_other),
          "distance" = c(distance_self, distance_other),
          "bin" = c(bin_self, bin_other),
          "angles" = c(angle_self, angle_other) ,
          stringsAsFactors = TRUE
        )
```

```
      dt[, val_sum := value1 + value2]
      dt[, val_dif := sqrt((value1 - value2) ** 2)]

    }

    #evaluate aggregate statistics

    aov_valDif <-
      aov(val_dif ~ social + fam, data = dt)
    aov_valSum <- aov(val_sum ~ social + fam, data = dt)
    aov_dist_by_bin <- aov(distance ~ bin, data = dt)

    p_values_valdDif <- summary(aov_valDif)[[1]]["Pr(>F)"]
    p_values_valSum <- summary(aov_valSum)[[1]]["Pr(>F)"]
    p_values_dist <- summary(aov_dist_by_bin)[[1]]["Pr(>F)"]

    p_values <-
      na.omit(c(p_values_valdDif, p_values_valSum, p_values_dist))

    print(summary(aov_valDif))
    print(summary(aov_valSum))
    print(summary(aov_dist_by_bin))

    if (all(p_values > alpha)) {
      break
    } else{
      next
    }
  }
  return(dt)
  }
}
```

R-Code for Randomization

```
randomisation_function <- function(dt, min_repetition_interval_stim = 3, max_
repetition_dim = 4,  max_repetition_fam = 4, nRuns = 4, block_length = 6 ) {


library(data.table)


  # Initialize variables and extract self and other data

  nTrial = nrow(dt)

  dt_self = dt[social == "self"]

  dt_other = dt[social == "other",]


  # Initialize empty list to store trial sequences for each run

  trials_full_dt = vector(mode = "list", length = nRuns)


  # Helper function to check if the interval between same stimuli is within t
he given limit

  interval_check <- function(trial_seq, stim, min_interval) {

    same_stim_ind = c(which(trial_seq$stim1 == stim), which(trial_seq$stim2 =
= stim))

    interval_size = abs(diff(same_stim_ind))

    return(any(interval_size < min_interval))

  }


  # Helper function to check if the repetition of a condition is within the g
iven limit

  repetition_check <- function(trial_seq, condition, max_repetition) {

    for (i in 1:nrow(trial_seq)) {

      repetition = (trial_seq[[condition]][i] == trial_seq[[condition]][(i+1)
:(i+max_repetition)])

      repetition[is.na(repetition)] = FALSE


      if (all(repetition)) return(TRUE)

    }

    return(FALSE)

  }
```

```
  # Iterate over runs
  for (r in 1:nRuns) {
    while (TRUE) {
      # Initialize trial sequence with original data
      trial_seq = dt

      # Shuffle self and other trials
      shuffled_s = dt_self[sample(1:nrow(dt_self)), ]
      shuffled_o = dt_other[sample(1:nrow(dt_other)), ]

      # Merge shuffled self and other trials into blocks
      for (b in seq(1, (nTrial/2), (block_length*2))) {
        if (b == 37) {
          trial_seq[b:(b+block_length-1),] = shuffled_s[b:(b+block_length-1),
]
          break
        }
        trial_seq[b:(b+block_length-1),] = shuffled_s[b:(b+block_length-1),]
        trial_seq[(b+block_length):(b+block_length+block_length-1),] = shuffl
ed_o[b:(b+block_length-1),]
      }

      # Merge shuffled self and other trials into blocks (second half)
      for (b in seq(1, (nTrial/2), (block_length*2))) {
        c = b + nTrial/2
        if (b == 37) {
          trial_seq[c:(c+block_length-1),] = shuffled_o[b:(b+block_length-1),
]
          break
        }
        b = b+block_length
        trial_seq[c:(c+block_length-1),] = shuffled_o[b:(b+block_length-1),]
        trial_seq[(c+block_length):(c+block_length+block_length-1),] = shuffl
ed_s[b:(b+block_length-1),]
      }
```

```
      # Check minimum repetition interval for same stimuli
      if (any(sapply(trial_seq$stim1, interval_check, trial_seq,
                     min_repetition_interval_stim)) ||
          any(sapply(trial_seq$stim2, interval_check, trial_seq,
                     min_repetition_interval_stim))) {
        next
      }
```

R-Code Behavioral analysis

```
library(data.table)
library(ggplot2)
library(ggrepel)
library(dplyr)
library(papaja)
library(ltm)
library(apaTables)


#-------------------------------------------------------------------------
--


# Accuracy


#-------------------------------------------------------------------------
--


# Calculate accuracy and aggregate statistics
accuracy_table <- dt[correct == 1, .N, by = .(task, sbj, session)]
accuracy_table[, too_slow := unique(dt[, too_slow, by = .(task, sbj, session)
]$too_slow)]


accuracy_table[, `:=` (
  errors = ifelse(task == "test", ntrial - (N + too_slow), ntrials_training -
(N + too_slow)),
  accuracy = N / (ifelse(task == "test", ntrials, ntrials_trinaing) - too_slo
w),
```

```
  mean = mean(accuracy),
  sd = sd(accuracy)
), by = .(task, sbj)]


accuracy_aggregate <- accuracy_table[, .(mean_accuracy = mean(accuracy), sd =
sd(accuracy)), by = .(session, task)]


# Plot accuracy
ggplot(accuracy_table, aes(x = session, y = mean, color = task)) +
  geom_point(aes(x = session, y = accuracy), position = position_jitterdodge(
jitter.width = 0.1, jitter.height = 0, dodge.width = 0.9), alpha = 0.4, size
= 2) +
  geom_line(aes(x = session, y = mean, group = task), position = position_dod
ge(width = 0.9), size = .5) +
  geom_point(position = position_dodge(width = 0.9), size = 4) +
  geom_errorbar(aes(x = session, ymin = mean - sd, ymax = mean + sd, group =
task), position = position_dodge(width = 0.9), size = 1, width = .4) +
  labs(title = "Accuracy", x = "Session", y = "Accuracy in %", color = "Task"
) +
  scale_fill_viridis_d(end = 0.80) +
  scale_color_viridis_d(end = 0.80) +
  theme(legend.position = "right", panel.background = element_blank(), panel.
grid = element_line(color = "gray"), panel.grid.minor.x = element_blank()) +
  geom_label_repel(data = accuracy_aggregate, aes(x = session, group = task,
y = mean_accuracy, label = round(mean_accuracy * 100)), size = 3, colour = "b
lack", position = position_dodge(width = 0.9), point.padding = 0.5, max.overl
aps = 20)


#------------------------------------------------------------------------
--


#Dimensionality


#------------------------------------------------------------------------
--


# Calculate accuracy by dimensionality
test_dt <- dt[task == "test"]
```

```
test_dt[, dimensionality := fcase(

  (mag_1 > mag__2 & prob_1 > prob_2) | (mag__2 > mag_1 & prob_2 > prob_1), "c
onsistent",

  (mag_1 != mag__2 & prob_1 == prob_2) | (mag_1 == mag__2 & prob_1 != prob_2)
, "1-dimensional",

  TRUE, "inconsistent"

)]


accuracy_condition <- test_dt[correct == 1, .N, by = .(sbj, dimensionality)]

accuracy_condition[, c("nCondition", "too_slow") := .(uniqueN(test_dt, by = .
(sbj, dimensionality)), unique(test_dt$too_slow))]

accuracy_condition[, `:=` (

  accuracy = N / nCondition,

  mean = mean(accuracy),

  sd = sd(accuracy)

), by = .(sbj, dimensionality)]


accuracy_condition_aggregate <- accuracy_condition[, .(mean_accuracy = mean(a
ccuracy), sd = sd(accuracy)), by = .(dimensionality)]

accuracy_condition_aggregate[, `:=` (

  se = sd / sqrt(length(accuracy)),

  t = qt(p = 0.05 / 2, df = length(accuracy) - 1, lower.tail = FALSE),

  margin_error = t * se

)]


# Plot accuracy by dimensionality

ggplot(accuracy_condition, aes(x = dimensionality, y = mean)) +

  geom_point(aes(y = accuracy), alpha = 0.4, size = 2) +

  geom_line(aes(y = mean, group = dimensionality), position = position_dodge(
width = 0.9), size = .5) +

  geom_point(position = position_dodge(width = 0.9), size = 4) +

  geom_errorbar(data = accuracy_condition_aggregate, aes(y = mean_accuracy, y
min = mean_accuracy - margin_error, ymax = mean_accuracy + margin_error, grou
p = dimensionality), position = position_dodge(width = 0.9), size = 1, width
= .4) +

  labs(title = "Accuracy by Dimensionality", x = "Dimensionality", y = "Accur
acy in %") +

  scale_fill_viridis_d(end = 0.80) +
```

```
  scale_color_viridis_d(end = 0.80) +

  theme(legend.position = "right", panel.background = element_blank(), panel.
grid = element_line(color = "gray"), panel.grid.minor.x = element_blank()) +

  geom_label_repel(data = accuracy_condition_aggregate, aes


#-------------------------------------------------------------------------
--


#Mann-Whitney U


#-------------------------------------------------------------------------
--


# perform Mann-Whitney test

mwu_results <- data.frame(matrix(ncol = 6, nrow = 0))


mwu_results <- rbind(mwu_results, c("accuracy", wilcox.test(accuracy ~ fam, d
ata = fam_dt, paired = FALSE, exact = TRUE, conf.int = TRUE)$statistic, wilco
x.test(accuracy ~ fam, data = fam_dt, paired = FALSE, exact = TRUE, conf.int
= TRUE)$p.value, NA, paste0("[", format(wilcox.test(accuracy ~ fam, data = fa
m_dt, paired = FALSE, exact = TRUE, conf.int = TRUE)$conf.int, digits = 2), "
]")))


mwu_results <- rbind(mwu_results, c("RT", wilcox.test(RT ~ fam, data = fam_dt
, paired = FALSE, exact = TRUE, conf.int = TRUE)$statistic, wilcox.test(RT ~
fam, data = fam_dt, paired = FALSE, exact = TRUE, conf.int = TRUE)$p.value, N
A, paste0("[", format(wilcox.test(RT ~ fam, data = fam_dt, paired = FALSE, ex
act = TRUE, conf.int = TRUE)$conf.int, digits = 2), "]")))

mwu_results <- rbind(mwu_results, c("inconclusiveness", wilcox.test(inconclus
iveness ~ fam, data = fam_dt, paired = FALSE, exact = TRUE, conf.int = TRUE)$
statistic, wilcox.test(inconclusiveness ~ fam, data = fam_dt, paired = FALSE,
exact = TRUE, conf.int = TRUE)$p.value, NA, paste0("[", format(wilcox.test(in
conclusiveness ~ fam, data = fam_dt, paired = FALSE, exact = TRUE, conf.int =
TRUE)$conf.int, digits = 2), "]")))


mwu_results <- rbind(mwu_results, c("high_confidence_proportion", wilcox.test
(high_confidence_proportion ~ fam, data = fam_dt, paired = FALSE, exact = TRU
E, conf.int = TRUE)$statistic, wilcox.test(high_confidence_proportion ~ fam,
data = fam_dt, paired = FALSE, exact = TRUE, conf.int = TRUE)$p.value, NA, pa
ste0("[", format(wilcox.test(high_confidence_proportion ~ fam, data = fam_dt,
paired = FALSE, exact = TRUE, conf.int = TRUE)$conf.int, digits = 2), "]")))
```

```
names(mwu_results) <- c("Dependent Variable", "U", "p-value", "Adjusted p-val
ue", "Confidence Interval")


# Bonferroni correction for multiple comparisons

mwu_results$`Adjusted p-value` <- p.adjust(mwu_results$'p-value', method = "b
onferroni")


names(mwu_results) <- c("Dependent Variable", "U", "p-value", "Adjusted p-val
ue", "Confidence Interval")


# Bonferroni correction for multiple comparisons

mwu_results$`Adjusted p-value` <- p.adjust(mwu_results$'p-value', method = "b
onferroni")


#-------------------------------------------------------------------------
--


#correlations


#-------------------------------------------------------------------------
--


# valdif - accuracy

biserial_cor <- biserial.cor(dt[session == 3]$valdif, dt[session == 3]$accura
cy, use = c("all.obs"), level = 2)


# valdif - confidence

biserial.cor(dt[session == 3,]$valdif, dt[session == 3,]$confidence_recode, u
se = c("all.obs"), level = 2)


cor_mat <- dt[session == 3, sum(correct)/.N, by = .(sbj)]

setnames(cor_mat, "V1", "accuracy")

cor_mat$high_confidence <- dt[session == 3, mean(confidence_recode), by = .(s
bj)][,2]

cor_mat$RT <- dt[session == 3, mean(rt), by = .(sbj)][,2]

cor_mat$inconclusiveness <- dt[session == 3, mean(inconclusiveness), by = .(s
bj)][,2]
```

```
apa.cor.table(
  cor_mat,
  filename = "./outputs/correlation_matrix.docx",
  table.number = NA,
  show.conf.interval = TRUE,
  show.sig.stars = TRUE,
  landscape = TRUE
)
```